

AD-A226 659

①

A Beam Pattern Design Procedure for Multidimensional Sonar Arrays Employing Minimum Variance Beamforming

by

Randall George Richards

B.S., Electrical Engineering  
Pennsylvania State University (1982)

Submitted in partial fulfillment of the requirements for the degree of

OCEAN ENGINEER

at the

MASSACHUSETTS INSTITUTE OF TECHNOLOGY

and the *N00123-89-G-0580*

WOODS HOLE OCEANOGRAPHIC INSTITUTION

September 1990

© Randall George Richards, 1990

DTIC  
ELECTE  
SEP 25 1990  
D CS

DTIC FILE COPY

NPS

Approved for public release  
Distribution Unlimited

The author hereby grants to MIT, WHOI and the U.S. Government permission to reproduce and to distribute copies of this thesis document in whole or in part.

Signature of Author ..... *Randall G. Richards* .....  
Joint Program in Oceanographic Engineering  
Massachusetts Institute of Technology  
Woods Hole Oceanographic Institution

Certified by ..... *Arthur B. Baggeroer* .....  
Dr. Arthur B. Baggeroer  
Professor of Ocean Engineering and Electrical Engineering  
Massachusetts Institute of Technology  
Thesis Supervisor  
August 10, 1990

Certified by ..... *James F. Lynch* .....  
Dr. James F. Lynch  
Associate Scientist  
Woods Hole Oceanographic Institution

Accepted by ..... *W. Kendall Melville* .....  
Dr. W. Kendall Melville  
Chairman, Joint Committee for Oceanographic Engineering  
Massachusetts Institute of Technology/Woods Hole Oceanographic Institution

90 09 24 051

**A Beam Pattern Design Procedure for Multidimensional Sonar  
Arrays Employing Minimum Variance Beamforming**

by

Randall George Richards

Submitted to the Massachusetts Institute of Technology/  
Woods Hole Oceanographic Institution  
Joint Program in Oceanographic Engineering  
on August 10, 1990, in partial fulfillment of the  
requirements for the degree of  
Ocean Engineer

**Abstract**

This paper develops a beam pattern design procedure for general multidimensional irregular sonar arrays that incorporates the not well understood effects of array geometry into the design process. The procedure is implemented by generating a "penalty function" in a spectral covariance function form. Processing the penalty function causes beam pattern high sidelobes to be penalized and the main lobe to be emphasized. This is accomplished by forming the penalty function in terms of an isotropic noise field of specified strength modified with a finite sector of low coherent energy and stabilized with incoherent sensor noise. By inputting the penalty function into a minimum variance beamformer, the beam pattern and aperture weights are calculated based on the given array geometry. The beamformer used is Capon's Maximum Likelihood Method. The array used to test the procedure is located on a sixty degree sector of a cylindrical surface. The procedure is implemented by two different methods, each with some desirable characteristics. One method suppresses sidelobes directly by the placement of nulls. The other method suppresses sidelobes indirectly by the enhancement of the main lobe with anti-nulls. Both methods are evaluated in terms of a sensitivity factor which constrains the maximum white noise array gain. Results show that both methods result in sidelobe levels that range from 20 to 35 dB lower compared to a conventional beam pattern with uniform aperture weighting and that the design procedure is applicable to beam patterns steered to both true broadside and to off-broadside directions.

Thesis Supervisor: Dr. Arthur B. Baggeroer  
Professor of Ocean Engineering and Electrical Engineering  
Massachusetts Institute of Technology

62  
1990

J

per form 50

A-1

## Acknowledgements

My two years as a graduate student have been an enjoyable and rewarding period. Many people have aided me in the course of my studies, more than I can reasonably mention here. However, there are a few people who deserve special mention.

First and foremost, I must thank my advisor, Dr. Arthur B. Baggeroer. Without his invaluable guidance, encouragement and patience, I would not have been able to successfully complete my studies. I must also thank Art for his concern and interest in my career.

A special thanks also goes to Eddie Scheer, computer wizard and musical guru. Eddie had to contend with numerous computer related questions and requests while maintaining, for the most part, his jovial attitude. In particular, Eddie was an available outlet when a break was needed and was an immense help when he typed a portion of this paper.

I am also indebted to Rob Fricke. Rob was the one person who was always available and always willing to discuss my studies and unrelated topics.

I must also recognize my fellow Joint Program adventurers. Although many of us had (and still have) the same goals, we have achieved those goals through different avenues and in doing so, have acquired a shared base of knowledge not found anywhere else.

I am most grateful to the United States Navy in conjunction with the Oceanographer of the Navy for allowing me this valuable opportunity and for provided the financial backing.

And last, I must recognize the love and support I have received from my family. My wife, Laurie, and my daughters, Brittany and Brianna, have kept me in touch with reality and my true priorities in life.

# Contents

<b>1</b>	<b>Introduction</b>	<b>9</b>
1.1	Background . . . . .	9
1.2	Objectives . . . . .	10
1.3	Overview . . . . .	11
<b>2</b>	<b>Problem Development</b>	<b>13</b>
2.1	Array Geometry . . . . .	13
2.2	Array Processing Approach . . . . .	15
2.2.1	Signal Model . . . . .	15
2.2.2	Spectral Covariance Matrix . . . . .	17
2.2.3	MLM Development . . . . .	21
2.2.4	Array Gain . . . . .	24
2.2.5	Spatial Scanning . . . . .	25
2.3	Beam Pattern Design Method . . . . .	29
2.3.1	Method A . . . . .	34
2.3.2	Method B . . . . .	35
2.4	Beamformer Performance Measures . . . . .	35
2.4.1	Eigenvalues . . . . .	35
2.4.2	Sensitivity Ratio . . . . .	37
2.4.3	Directivity Index . . . . .	38
<b>3</b>	<b>Beamforming Results</b>	<b>40</b>
3.1	Preliminaries . . . . .	40

3.2	Broadside Results . . . . .	41
3.2.1	Method A . . . . .	45
3.2.2	Method B . . . . .	52
3.3	Steered Results . . . . .	59
3.3.1	Method A . . . . .	64
3.3.2	Method B . . . . .	64
4	Summary and Conclusions	74
A	Spectral Covariance Matrix Inversion	78
B	Dolph-Chebyshev Weights	81

# List of Figures

2-1	Array Geometry . . . . .	14
2-2	Array Coordinate System and Dimensions . . . . .	14
2-3	Element Numbering Scheme . . . . .	19
2-4	Spectral Covariance Matrix . . . . .	20
2-5	System Architecture for a 200 Element Array . . . . .	23
2-6	Projected Scanning Vector Locations. Every other scanning increment in elevation and azimuth is shown. The shading illustrates the variability in azimuth of the spatial separation between scan directions relative to the spatial separation at broadside resulting from the uniform angular scanning implementation. . . . .	28
2-7	Null Placement Effects. For a source (solid line) incident at some $\mathbf{k}$ , the MVDP beamformer optimally places a null in the array response pattern (dashed line) in the direction of the source incident at $\mathbf{k}$ . . . . .	30
2-8	Three Dimensional Mesh Plot of Penalty Function . . . . .	32
2-9	Overhead View of Penalty Function . . . . .	33
2-10	Two Dimensional Cross Section of Penalty Function . . . . .	33
3-1	array output for plane wave case . . . . .	42
3-2	conventional beam pattern steered to $0^\circ$ elevation and $90^\circ$ azimuth . . . . .	43
3-3	conventional beam pattern steered to $0^\circ$ elevation and $102^\circ$ azimuth . . . . .	44
3-4	Eigenvalue Performance Results for Case 11A . . . . .	47
3-5	array output for case 11A, $\lambda_{min} = 10^{-3}$ . . . . .	48
3-6	beam pattern for case 11A, $\lambda_{min} = 10^{-3}$ . . . . .	49

3-7	square magnitude of element weights, case 11A, $\lambda_{min} = 10^{-3}$ . . . . .	50
3-8	corrected phase of element weights, case 11A, $\lambda_{min} = 10^{-3}$ . . . . .	51
3-9	Eigenvalue Performance Results for Case 9B . . . . .	53
3-10	array output, case 9B, $\lambda_{min} = 10^{-4}$ . . . . .	55
3-11	beam pattern, case 9B, $\lambda_{min} = 10^{-4}$ . . . . .	56
3-12	square magnitude of element weights, case 9B, $\lambda_{min} = 10^{-4}$ . . . . .	57
3-13	corrected phase of element weights, case 9B, $\lambda_{min} = 10^{-4}$ . . . . .	58
3-14	array output, case 5B, $\lambda_{min} = 10^{-4}$ . . . . .	60
3-15	beam pattern, case 5B, $\lambda_{min} = 10^{-4}$ . . . . .	61
3-16	square magnitude of element weights, case 5B, $\lambda_{min} = 10^{-4}$ . . . . .	62
3-17	corrected phase of element weights, case 5B, $\lambda_{min} = 10^{-4}$ . . . . .	63
3-18	array output, steered method A penalty function . . . . .	65
3-19	beam pattern, steered method A penalty function . . . . .	66
3-20	square magnitude of element weights, steered method A penalty function . . . . .	67
3-21	corrected phase of element weights, steered method A penalty function . . . . .	68
3-22	array output, steered method B penalty function . . . . .	70
3-23	beam pattern, steered method B penalty function . . . . .	71
3-24	square magnitude of element weights, steered method B penalty function . . . . .	72
3-25	corrected phase of element weights, steered method B penalty function . . . . .	73
4-1	Plot of First Sidelobe versus Center Region Width, Method A. Conventional main lobe widths in terms of angular separation between first nulls are approximately 24° in azimuth and 50° in elevation. . . . .	75
4-2	Plot of First Sidelobe versus Center Region Width, Method B. Conventional main lobe widths in terms of angular separation between first nulls are approximately 24° in azimuth and 50° in elevation. . . . .	76
B-1	Dolph-Chebyshev square magnitude element weights . . . . .	82

# List of Tables

2.1	Summary of Computational Requirements for Different Scan Patterns . . .	27
3.1	Penalty Function Parameters . . . . .	45
3.2	Minimum Eigenvalues and Associated Dynamic Ranges Tested for Method A Penalty Functions . . . . .	46
3.3	Method A Case Study Summary . . . . .	47
3.4	Minimum Eigenvalues and Associated Dynamic Ranges Tested for Method B Penalty Functions . . . . .	53
3.5	Method B Case Study Summary . . . . .	54
A.1	Computational Times for Matrix Solution Methods . . . . .	79

# Chapter 1

## Introduction

### 1.1 Background

The problem of beamforming with multidimensional arrays is a very important problem with numerous applications, yet it is not well understood. Whereas one dimensional, equally spaced arrays have many formulations and solutions based on extensive temporal analysis, arrays with added dimensions and nonuniform spacing introduce unique problems and possibilities which have no direct temporal equivalent.[1] In terms of the bearing estimation problem which is addressed in this investigation conventional beamforming can be described as the shading or windowing of array sensor data to obtain a desirable directional scan pattern, or beam pattern. One dimensional windows are numerous and well documented.[2] In two dimensional and higher dimensional cases, fewer windows are available.[3] The majority of the multidimensional windows are based either on a perfect circular based symmetric geometry (a perfect sphere or cylinder) or on the extension of one dimensional windows to higher dimensions which routinely requires uniformly sampled apertures.[4,5] Unfortunately, all multidimensional arrays are not completely circular and/or do not have regular sensor spacing. The impact of array geometry, particularly in three dimensions, on the spectral estimation and bearing estimation problems is not well understood.[6] Therefore, the purpose of this investigation is to develop a beam pattern design procedure that can be used on general multidimensional irregular arrays which includes the effects of the array geometry. The design procedure uses a data-adaptive,

minimum variance method that can be applied to arrays with nonuniform spacing. The minimum variance procedure is Capon's High Resolution Frequency Wavenumber Estimation Method more commonly known as the Maximum Likelihood Method (MLM). [7] The test array, which has proposed applications in an undersea environment, consists of a three dimensional sonar array located on an arc of a cylindrical surface. The primary objective is to design beam patterns by processing array data with the MLM beamformer. The source of array data is the design tool and is contained in a special spectral covariance matrix termed a "penalty function." Generation of the penalty function is the important issue of the design procedure and is the focus of this investigation.

## 1.2 Objectives

As previously stated, the primary objective is to develop a beam pattern design procedure using an MLM beamformer that can be used on irregular arrays where traditional aperture shadings are not applicable. This primary objective results in two issues:

- can the MLM beamformer be effectively used in a design role?
- can the MLM beamformer control sidelobes?

Both of these issues are examined using the penalty function concept. Selection of the proper penalty function results in a beam pattern with low sidelobes when compared to a conventional beam pattern generated from a uniform aperture shading. Different penalty functions result in beam patterns with different sidelobes. The selection of different penalty functions gives the designer control over the procedure. In applying this procedure the designer obtains a qualitative perception of the array's performance in terms of the array geometry and element spacing which aids in the design process.

To aid in the analysis and the evaluation of the primary objective, quantitative measures of array performance in terms familiar to conventional beamforming are included. The two performance measures relied upon are directivity index and sensitivity ratio. Sensitivity ratio is a relative measure of white noise array gain or array sensitivity. The quantitative measure used to describe the penalty function in terms of array performance is the minimum eigenvalue of the penalty function. One additional aid is a comparison of

the shading obtained by the design procedure with the aperture shading resulting from a Dolph-Chebyshev design for a uniform rectangular array. The quantitative performance measures and Dolph-Chebyshev comparison study enable an analysis and evaluation based on proven conventional methods and parameters.

The array application used in this investigation deals with a large array composed of 200 elements in a three dimensional sound field. Arrays with a large number of elements (as is the case here) lead to computationally complex and time intensive array processing requirements; therefore, a significant issue concerns obtaining an implementation which reduces or limits the computational complexity and processing times. In order to limit the processing requirements, the aspects of directional (baffled) hydrophones or sensors, array structural shading and the estimation process of the spectral covariance matrix are not considered. The array structure is transparent to sound from any direction and the spectral covariance matrix is assumed to be available. The procedure is based on a plane wave development. Since the MLM requires a matrix inverse, even the use of these simplifications still leads to a time intensive process. In an effort to further reduce processing times, the investigation highlights a comparison of two matrix solution methods:

- Gaussian elimination
- a Toeplitz bordering approach based on Levinson's method.[8]

### 1.3 Overview

The remainder of this paper is divided into three chapters and two appendices. Chapter 2 describes the problem and is broken into four additional sections.

- Section 2.1 describes the array geometry.
- Section 2.2 defines the signal model, develops the spectral covariance matrix and its properties, reviews conventional beamforming and MLM beamforming, defines array gain and develops the spatial scanning problem.
- Section 2.3 develops the penalty function.

- Section 2.4 develops and defines the beamformer performance measures.

Chapter 3 contains the beamforming design results. The design results are split into three sections.

- Section 3.1 includes beamformer verification results which are useful as points of comparison.
- Section 3.2 contains extensive results on broadside beam pattern designs.
- Section 3.3 contains results of steered beam pattern designs.

Chapter 4 contains a summary.

Appendix A contains timing data resulting from the investigation of the Gaussian elimination and Toeplitz bordering matrix solution methods.

Finally, appendix B contains a comparison of the aperture shading design results with the traditional Dolph-Chebyshev design procedure.

## Chapter 2

# Problem Development

### 2.1 Array Geometry

The array used in this investigation has proposed applications on submersible bodies. It is located on a 60 degree arc of a cylindrical surface. The array is shown in figure 2-1 and is to be operationally oriented as depicted. The array has intrinsic structure but is neither linear nor circular. The array is to be applied in a manner which reduces the problem to processing only the half space on the same side of the cylinder on which the array is located.

The array consists of 200 elements arranged in ten rows (or lines) of twenty elements each. Considered separately, each line of twenty elements is identical. The array is symmetric about the x and z axes for the coordinate system defined in figure 2-2. This structure leads to some important results when considering the spectral covariance matrix.

The design wavelength is defined as the wavelength ( $\lambda$ ) that determines the element spacing. All of the work performed in the investigation of this array is accomplished at the design wavelength; therefore, design wavelength and  $\lambda$  are interchangeable. The element spacing is specified to be one quarter of the design wavelength or  $\lambda/4$ . All dimensions of the array (including the cylinder radius) are related in terms of the design wavelength.

The structure of the array can be compared to a simpler two dimensional planar array. This comparison is valuable because uniform planar arrays are well documented. In order to prove this comparison is justified to first order, the extent the actual three dimensional

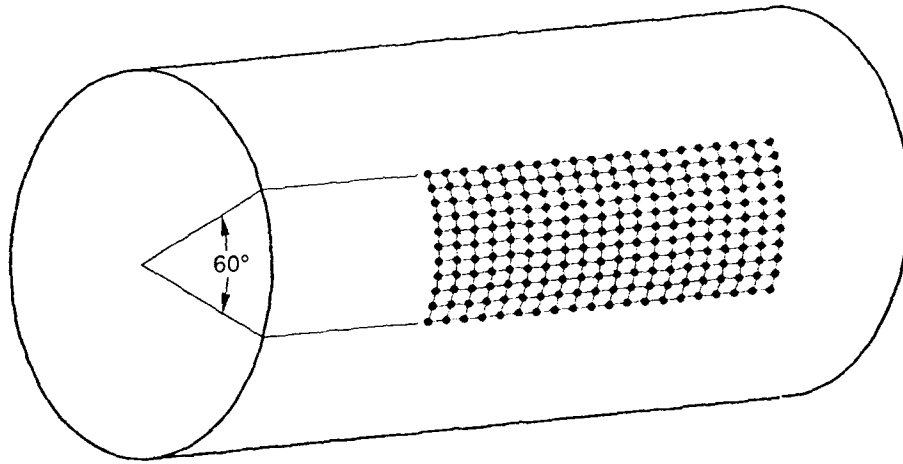


Figure 2-1: Array Geometry

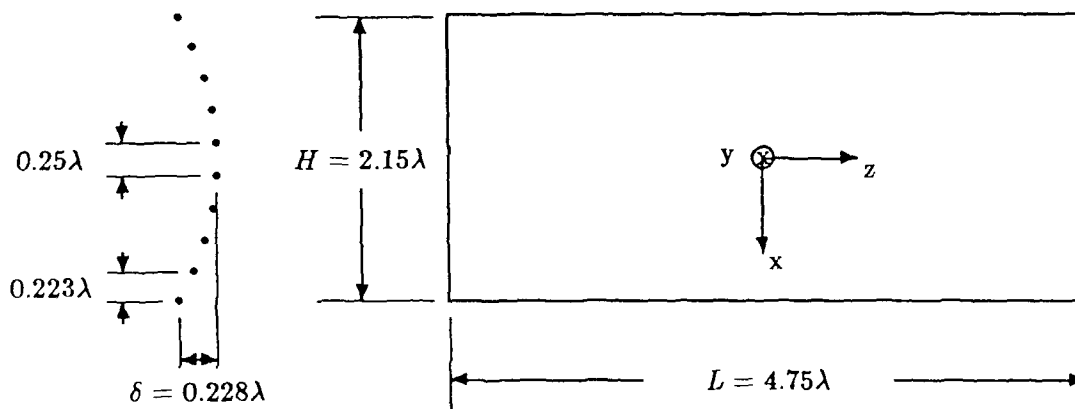


Figure 2-2: Array Coordinate System and Dimensions

array deviates from a true uniform planar array must be determined. If the array is considered to be a structure of ten 20 element line arrays, then the length (L) of the line arrays is  $4.75\lambda$ . If the angular separation of the line arrays is uniform and the arc length of this angular separation is approximately linear and equal to  $\lambda/4$ , then the relationship between R and  $\lambda$  can be determined by equating the arc length of the 60 degree sector to the arc length encribed by the 10 line arrays. This results in

$$\frac{\pi}{3}R = 9\frac{\lambda}{4} \quad (2.1)$$

or

$$R = \frac{27}{4\pi}\lambda \quad (2.2)$$

By applying some simple trigonometry, the planar height (H) of the array as projected onto the x-z plane is equal to the radius R, or  $2.15\lambda$ . The maximum deflection of the array (or a measure of the curvature from the x-z plane) is approximately equal to  $0.288\lambda$ . The projected vertical spacing in the array center is equal to  $0.25\lambda$  and is approximately equal to  $0.223\lambda$  at the array top or bottom. A pictorial explanation of these dimensions is illustrated in figure 2-2. The projected array has uniform spacing along the axial (or z) axis and nonuniform spacing in the x direction (although the spacing is nearly uniform.) Therefore, the three dimensional array can be approximated by a uniform rectangular array if the effects of curvature are neglected. The rectangular array approximation is better in the axial direction; therefore, the expectation is that design results in the axial direction will more closely resemble results of the uniform rectangular array. The rectangular array comparison provides a reasonable model which is useful in establishing an intuitive feel for the expected performance of the test array.

## 2.2 Array Processing Approach

### 2.2.1 Signal Model

One purpose of an array and its associated processor is to provide an estimate of the directional spectrum of a space/time stochastic process. The directional spectrum

information is contained in the frequency wavenumber function. To understand the array processing system the signal model must first be defined. The space/time stochastic processes being considered are assumed to be temporally wide sense stationary (defined in reference [9]) and spatially homogeneous (defined in reference [1].) The wide sense stationarity assumption implies that disjoint frequency bands are uncorrelated. The spatial homogeneity assumption implies that disjoint wavenumber bands or directions are uncorrelated, i. e. no correlated multipaths. Both the wide sense stationarity and spatial homogeneity assumptions are not universally valid in the ocean environment, but can be closely approximated in practice by proper choices of time and space scales. Although time domain analysis is not addressed in this study and the actual physical dimensions of the array are not known, the wide sense stationarity and spatial homogeneity assumptions are presumed to be valid based on anticipated time and spatial scales. The space/time stochastic processes are represented in a Stieltjes integral form [10] as

$$x(t, \mathbf{z}) = \int_{-\infty}^{\infty} \int_{-\infty}^{\infty} \int_{-\infty}^{\infty} e^{j(2\pi f t - \mathbf{k} \cdot \mathbf{z})} dX(f, \mathbf{k}) \quad (2.3)$$

where  $t$  is the time argument,  $\mathbf{z}$  is the vector representing the spatial position and  $\mathbf{k}$  is the three dimensional wavenumber vector.<sup>1</sup> For the wide sense stationary and spatially homogeneous processes considered,  $X(f, \mathbf{k})$  defines a Fourier transform representation for a plane wave of frequency  $f$  and wavenumber vector  $\mathbf{k}$ . Thus  $x(t, \mathbf{z})$  is composed of a superposition of plane waves  $X(f, \mathbf{k})$ . [1] For the three dimensional ocean environment,  $f$  and  $\mathbf{k}$  must satisfy the dispersion relation

$$|\mathbf{k}| = 2\pi f/c \quad (2.4)$$

Equation 2.4 results from the three dimensional wave equation where  $c$  is the speed of sound in water. This dispersion relation corresponds to free space propagation. The space/time covariance function  $K(t, t-\tau, \mathbf{z}, \mathbf{z}-\Delta\mathbf{z})$  is the cross correlation of the stochastic process at times  $t$  and  $t-\tau$  and spatial positions  $\mathbf{z}$  and  $\mathbf{z}-\Delta\mathbf{z}$ . All processes are assumed

---

<sup>1</sup>Lower case letters are used to depict temporal representations while upper case letters depict transform representations. Similarly, upper case bold face letters represent matrices and lower case bold face letters represent vectors.

to be zero mean stochastic processes.  $K_x(t, t - \tau, \mathbf{z}, \mathbf{z} - \Delta \mathbf{z})$  is determined by

$$K_x(t, t - \tau, \mathbf{z}, \mathbf{z} - \Delta \mathbf{z}) = E[x(t, \mathbf{z})x^*(t - \tau, \mathbf{z} - \Delta \mathbf{z})] \quad (2.5)$$

where \* denotes complex conjugate and  $E$  represents the ensemble expectation operator. The frequency domain representation of the space/time covariance function is the spectral covariance function  $S_x(f, \mathbf{z}, \mathbf{z} - \Delta \mathbf{z})$  which is defined as

$$S_x(f, \mathbf{z}, \mathbf{z} - \Delta \mathbf{z}) = \int_{-\infty}^{\infty} K_x(t, t - \tau, \mathbf{z}, \mathbf{z} - \Delta \mathbf{z}) e^{-j2\pi f\tau} d\tau \quad (2.6)$$

$S_x(f, \mathbf{z}, \mathbf{z} - \Delta \mathbf{z})$  represents the cross spectra between positions (corresponding to array elements)  $\mathbf{z}$  and  $\mathbf{z} - \Delta \mathbf{z}$ . The frequency wavenumber representation of the space/time stochastic process, called the frequency wavenumber function  $P(f, \mathbf{k})$ , is defined as

$$P(f, \mathbf{k}) = \int \int \int_{-\infty}^{\infty} S_x(f, \mathbf{z}, \mathbf{z} - \Delta \mathbf{z}) e^{j\mathbf{k} \cdot \Delta \mathbf{z}} d(\Delta \mathbf{z}) \quad (2.7)$$

Since  $f$  and  $|\mathbf{k}|$  are related by equation 2.4, fixing  $f$  reduces the problem to determining the direction of propagation of  $|\mathbf{k}|$ . This is the approach used throughout this study;  $f$  is fixed and then the half space in which the array resides is scanned to determine the direction of propagation parameterized in terms of an bearing in azimuth and an elevation angle. The estimate of the direction of propagation or directional spectrum, embedded in the function  $P(f, \mathbf{k})$ , is the desired output of the array processor.

### 2.2.2 Spectral Covariance Matrix

An examination of the spectral covariance matrix is included at this point because it aids in the understanding of the beamforming procedure and also reveals some pertinent characteristics of the matrix operations which are encountered.

The spectral covariance matrix can be decomposed into two components, one coherent and one incoherent, by setting (dropping arguments for brevity)<sup>2</sup>

$$\mathbf{S}_x = \sigma_S^2 \mathbf{d} \mathbf{d}^\dagger + \sigma_N^2 \mathbf{Q} \quad (2.8)$$

---

<sup>2</sup>† represents complex conjugate transpose

where

$$\mathbf{d} = \begin{bmatrix} e^{j\mathbf{k}_s \cdot \mathbf{z}_1} \\ \vdots \\ e^{j\mathbf{k}_s \cdot \mathbf{z}_N} \end{bmatrix} \quad (2.9)$$

is the geometric phase or direction vector of a plane wave signal propagating with wavenumber vector  $\mathbf{k}_s$  and signal strength  $\sigma_S^2$ .  $\mathbf{Q}$  represents the normalized (trace  $\mathbf{Q} = N$ ) noise cross spectral density matrix of element outputs with noise strength  $\sigma_N^2$ . If the noise consists solely of uncorrelated components, then  $\mathbf{Q}$  reduces to the identity matrix  $\mathbf{I}$ .

The coherent input places the restrictions on  $f$  and  $\mathbf{k}_s$  found in equation 2.4. The coherent input used in this study consists of plane waves which are modeled at time  $t$  and position  $\mathbf{z}$  as

$$x(t, \mathbf{z}) = a(f) e^{j(2\pi ft - \mathbf{k}_s \cdot \mathbf{z})} \quad (2.10)$$

where  $a(f)$  is a frequency dependent amplitude function. The coherent component of the spectral covariance matrix resulting from the plane wave input (determined by applying equations 2.5 and 2.6) is

$$\sigma_S^2 \mathbf{d} \mathbf{d}^\dagger = \sigma_S^2 e^{-j\mathbf{k}_s \cdot \Delta \mathbf{z}_{i,j}} \quad \forall i, j \quad (2.11)$$

where  $\sigma_S^2$  is frequency dependent and  $\Delta \mathbf{z}_{i,j} = \mathbf{z}_i - \mathbf{z}_j$  corresponds to the vector difference between the  $i^{\text{th}}$  and  $j^{\text{th}}$  elements. The exponential argument  $\mathbf{k}_s \cdot \Delta \mathbf{z}_{i,j}$  represents the phase delay due to propagation of the plane wave between the  $i^{\text{th}}$  and  $j^{\text{th}}$  elements.

The first observation deals with the structure of a matrix formed by equation 2.8. Matrices of this form are Hermitian symmetric or simply Hermitian. A Hermitian matrix is defined by  $\mathbf{S} = \mathbf{S}^\dagger$ . The second observation results after examining equation 2.11. The coherent input is dependent only on the difference in element positions. This spatial homogeneity leads to an embedded Toeplitz structure. A Toeplitz matrix is defined as a matrix whose  $ij$ th element  $s(i, j)$  is a function of  $(i-j)$  and thus has identical elements along the main diagonal and each of the subdiagonals. (Reference [11] contains an excellent summary of Hermitian and Toeplitz matrix properties.) To fully see the structure of the matrix formed by equation 2.11 for the test array, consider an element identification scheme where the elements are numbered consecutively along each successive row (or line) starting at the array top. This numbering scheme is shown in figure 2-3. The spectral

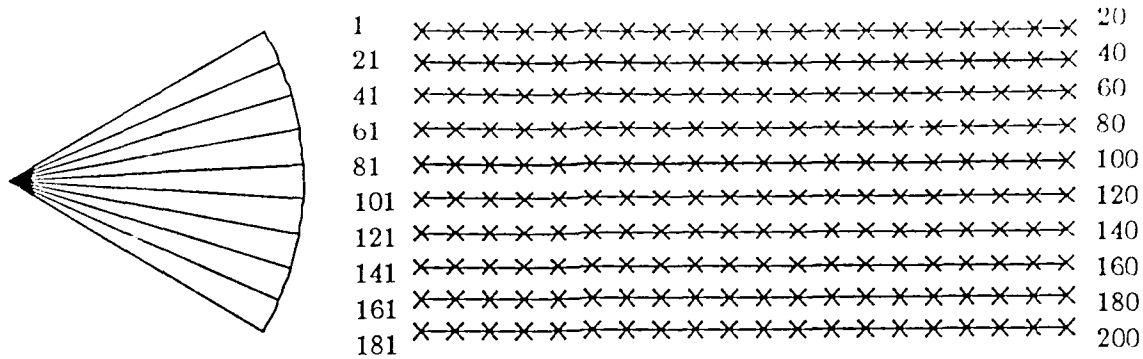


Figure 2-3: Element Numbering Scheme

covariance matrix resulting from this numbering scheme is shown in figure 2-4 where the matrix is partitioned to indicate specific sub-matrices. Each  $s_{k,l}$  corresponds to the cross spectral covariance of the  $k$ th element with the  $l$ th element. Each sub-matrix corresponds to the spectral covariance formed between elements located in two of the line arrays. The main diagonal of sub-matrices is the result of forming the spectral covariance of each line array with itself; the main diagonal sub-matrices are all identical because each line array is identical and the coherent input is perfectly correlated.

$S_z$  can also be represented as a two level matrix where to the first order level

$$S_z = \begin{bmatrix} S_{1,1} & S_{1,2} & \cdots & S_{1,10} \\ S_{2,1} & S_{2,2} & & \\ \vdots & & \ddots & \\ S_{10,1} & & & S_{10,10} \end{bmatrix} \quad (2.12)$$

Each sub-matrix  $S_{i,j}$  is the cross covariance between the  $i$ th and  $j$ th line arrays and is defined in figure 2-4 by each partition. For example  $S_{1,2}$  is the sub-matrix in the partitioned first row and second column of figure 2-4 and is formed from the line array with elements 1 through 20 and the line array with elements 21 through 40. The spectral covariance matrix has several distinctive characteristics.

- $S_z$  is  $N \times N$  (or  $200 \times 200$  for the test array.)
- Each sub-matrix,  $S_{i,j}$ , is Toeplitz and Hermitian
- $S_z$ , to the first order level, is Hermitian but not Toeplitz because of the vertical

$s_{1,1}$	$s_{1,2}$	...	$s_{1,20}$	$s_{1,21}$	$s_{1,22}$	...	$s_{1,40}$	$s_{1,181}$	$s_{1,182}$	...	$s_{1,200}$
$s_{2,1}$	$s_{2,2}$	...		$s_{2,21}$	$s_{2,22}$	...		$s_{2,181}$	$s_{2,182}$	...	
$\vdots$	$\vdots$	$\ddots$		$\vdots$	$\ddots$	$\ddots$		$\vdots$	$\ddots$	$\ddots$	
$s_{20,1}$			$s_{20,20}$	$s_{20,21}$			$s_{20,40}$	$s_{20,180}$			$s_{20,200}$
$s_{21,1}$	$s_{21,2}$	...	$s_{21,20}$	$s_{21,21}$	$s_{21,22}$	...	$s_{21,40}$				
$s_{22,1}$	$s_{22,2}$	...		$s_{22,21}$	$s_{22,22}$	...					
$\vdots$	$\vdots$	$\ddots$		$\vdots$	$\ddots$	$\ddots$					
$s_{40,1}$			$s_{40,20}$	$s_{40,21}$			$s_{40,40}$				
$\vdots$	$\vdots$	$\ddots$									
$s_{181,1}$	$s_{181,2}$	...	$s_{181,20}$					$s_{181,181}$	$s_{181,182}$	...	$s_{181,200}$
$s_{182,1}$	$s_{182,2}$	...						$s_{182,181}$	$s_{182,182}$	...	
$\vdots$	$\vdots$	$\ddots$						$\vdots$	$\ddots$	$\ddots$	
$s_{200,1}$			$s_{200,20}$					$s_{200,181}$			$s_{200,200}$

$S_z =$

Figure 2-4: Spectral Covariance Matrix

structure of the array. However, the main diagonal is a constant (to the first order level.)

- The addition of the incoherent term will not change the embedded Toeplitz structure of the sub-matrices.

Matrices with the form of  $S_x$  are frequently classified as a two level matrices. References [12] and [13] include a complete discussion on the classification of matrices in this manner.  $S_x$  in this case is classified as a Hermitian-Toeplitz two level matrix, but by permuting corresponding rows and columns, the matrix can be transformed into a Toeplitz-Hermitian two level matrix where the first level is Toeplitz and the second level sub-matrices are Hermitian. This is important because there currently exist efficient and documented algorithms which can invert a Toeplitz-Hermitian two level matrix.[13] As is shown later the spectral covariance matrix needs to be inverted. Details of the matrix inversion selection process are included in Appendix A. (This selection process played a very important role in this investigation; the time intensive inversion process had a direct relationship to the processing time.)

### 2.2.3 MLM Development

In the context of this investigation array processing and beamforming are synonymous. There is much literature on beamforming, both conventional and data adaptive. Complete reviews of processing methods are readily available.[14] Since the purpose of this study is to develop a beam pattern design procedure that can be applied to nonuniform multidimensional arrays, the choice of usable methods is limited to the MLM beamformer. The procedure can be more accurately described as a minimum variance, distortionless processor (sometimes referred to as MVDP).[6] From this point on, the beamformer will be referred to as the MVDP because it more accurately describes the processor. What follows is a development of conventional beamforming and the MVDP.

$w(f|k_T)$  is the aperture weighting function with the processor steered to  $k_T$ .<sup>3</sup> For the sampled aperture consisting of an N element array, the  $i^{th}$  component of  $w$  is the complex

---

<sup>3</sup>The development is the same as used in reference [1].

conjugate of the  $i^{th}$  element's weighting ( $w_i^*$ ).

$$\mathbf{w}(f | \mathbf{k}_T) = \begin{bmatrix} \vdots \\ w_i^*(f | \mathbf{k}_T) \\ \vdots \end{bmatrix} \quad (2.13)$$

The aperture weighting function, or weighting vector, can also be considered to be an n-dimensional taper or shading function for an n-dimensional array. It should be observed that  $\mathbf{w}$  is dependent on the steer direction and can be complex. The scanning vector  $\mathbf{e}(\mathbf{k}_T)$  steered to  $\mathbf{k}_T$  is defined as

$$\mathbf{e}(\mathbf{k}_T) = \begin{bmatrix} e^{j\mathbf{k}_T \cdot \mathbf{z}_1} \\ \vdots \\ e^{j\mathbf{k}_T \cdot \mathbf{z}_N} \end{bmatrix} \quad (2.14)$$

where again  $\mathbf{z}_i$  is the  $i^{th}$  element's position vector of an N element array. The scanning vector can be interpreted as the plane wave phase delays which must be applied to the array elements to steer the array in the direction of  $\mathbf{k}_T$ . The scanning vector also has an interpretation of being a replica field or the field at the array produced by a source at some position in the water column.

The output of the array beam steered to  $\mathbf{k}_T$  is defined in conventional beamforming as

$$Y(f, \mathbf{k}_T) = \mathbf{w}^\dagger \mathbf{X} = \sum_{i=1}^N w_i(f | \mathbf{k}_T) X(f, \mathbf{z}_i) \quad (2.15)$$

This system architecture is depicted in figure 2-5. The array response pattern  $\mathcal{W}(f, \mathbf{k} | \mathbf{k}_T)$  is given by

$$\mathcal{W}(f, \mathbf{k} | \mathbf{k}_T) = \mathbf{w}^\dagger \mathbf{e} = \sum_{i=1}^N w_i(f | \mathbf{k}_T) e^{j\mathbf{k} \cdot \mathbf{z}_i} \quad (2.16)$$

and represents the response of the array (steered in the direction of  $\mathbf{k}_T$ ) over the aperture to a plane wave signal. If  $\mathbf{k}$  is fixed and the function  $\mathcal{W}(f, \mathbf{k} | \mathbf{k}_T)$  is evaluated over a spatial region, then the beam pattern B is obtained where

$$B(f, \theta, \phi | \mathbf{k}_T) = \mathcal{W}(f, \mathbf{k} | \mathbf{k}_T) \Big|_{\mathbf{k} = \frac{2\pi}{\lambda} \mathbf{a}(\theta, \phi)} \quad (2.17)$$

where  $\lambda$  is the wavelength and  $\mathbf{a}(\theta, \phi)$  is a unit vector specified in a spherical geometry.

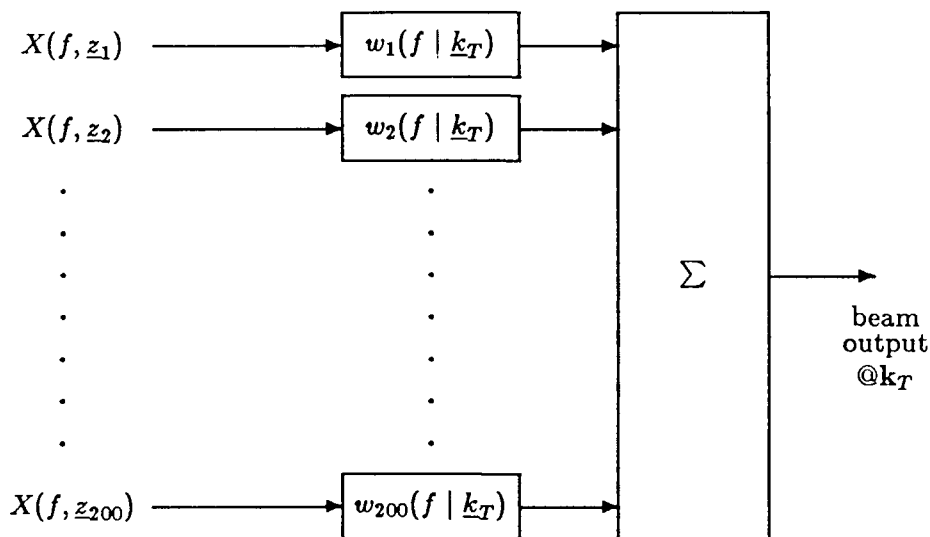


Figure 2-5: System Architecture for a 200 Element Array

Because  $P(f, \mathbf{k})$  is a measure of power, this leads to a representation of the response of the array as a function of two array sensor locations. This will result in a second moment representation for the array output and requires a second moment input. The array input is the spectral covariance function  $S_x(f, \mathbf{z}_i, \mathbf{z}_j)$  as defined by equation 2.6. The output of the beam steered to  $\mathbf{k}_T$  is the power density spectrum  $S_y(f|\mathbf{k}_T)$  and is given by

$$S_y(f|\mathbf{k}_T) = \mathbf{w}^\dagger(f|\mathbf{k}_T) \mathbf{S}_x(f, \mathbf{z}_i, \mathbf{z}_j) \mathbf{w}(f|\mathbf{k}_T) \quad (2.18)$$

$S_y(f|\mathbf{k}_T)$ , as defined by equation 2.18, is the output of a conventional beamformer and is the estimate of  $P(f, \mathbf{k})$  with the array steered to  $\mathbf{k}_T$ . The MVDP is obtained by minimizing the response of equation 2.18 (minimum variance) subject to unity gain in the look direction (distortionless response.) The MVDP solutions are [1,7,15]

$$\mathbf{w}_{MVDP}(f|\mathbf{k}_T) = \frac{\mathbf{S}_x^{-1} \mathbf{e}(\mathbf{k}_T)}{\mathbf{e}^\dagger(\mathbf{k}_T) \mathbf{S}_x^{-1} \mathbf{e}(\mathbf{k}_T)} \quad (2.19)$$

$$W_{MVDP}(f, \mathbf{k}|\mathbf{k}_T) = \frac{\mathbf{e}^\dagger(\mathbf{k}) \mathbf{S}_x^{-1} \mathbf{e}(\mathbf{k}_T)}{\mathbf{e}^\dagger(\mathbf{k}_T) \mathbf{S}_x^{-1} \mathbf{e}(\mathbf{k}_T)} \quad (2.20)$$

$$S_{y, MVDP}(f|\mathbf{k}_T) = \frac{1}{\mathbf{e}^\dagger(\mathbf{k}_T) \mathbf{S}_x^{-1} \mathbf{e}(\mathbf{k}_T)} \quad (2.21)$$

The MVDP method adaptively finds different aperture weightings for different input signal fields such that sidelobes are adjusted to reject interfering coherent noise sources and the incoherent noise. This method is optimum in the sense that it minimizes the array response over the aperture of the noise field (the input signal not in the beam) by design and application of a spatial filter. This spatial filter estimates the power in a plane wave propagating with frequency  $f$  and wavenumber vector  $\mathbf{k}_T$  in the presence of interfering plane waves and sensor noise.[16] To fully define the directional spectrum, the signal field must be scanned over the appropriate angular space (which, for this study, is the half space in which the test array is located.) If only uncorrelated noise is present, then uniform weighting with the conventional beamformer is optimal.

#### 2.2.4 Array Gain

Array gain is the improvement in signal to noise ratio due to beamforming. This is a result of finite beam widths rejecting noise and signals not in the beam. Ideally, for the signal of interest, signal rejection is small while the noise rejection is large resulting in a large array gain. The array gain as such is defined as

$$G = \frac{|\mathbf{w}^\dagger \mathbf{d}|^2}{\mathbf{w}^\dagger \mathbf{Q} \mathbf{w}} \quad (2.22)$$

which is simply the ratio of the signal response to the noise response. In the context of the MVDP processor, the optimum array gain is [1,17]

$$G_{opt} = \mathbf{e}^\dagger \mathbf{Q}^{-1} \mathbf{e} \quad (2.23)$$

For the case of spatially white or sensor noise with omnidirectional sensors, the array gain becomes the white noise gain or

$$G_w = \frac{|\mathbf{w}^\dagger \mathbf{d}|^2}{\mathbf{w}^\dagger \mathbf{w}} \leq N \quad (2.24)$$

where  $N$  is the number of sensors. Equality occurs when the processor is perfectly matched and there is uniform weighting. The processor is defined to be perfectly matched to the signal directional characteristics when  $\mathbf{e} = \mathbf{d}$  where  $\mathbf{d}$  is defined by equation 2.9.[17] Mismatch occurs whenever  $\mathbf{e} \neq \mathbf{d}$  and may, for example, be caused by non-plane wave

propagation, errors associated with the sensors, sampling, quantization, and steering off of the signal direction. When the errors due to mismatch are uncorrelated, the sensitivity ( $S_w$ ) of the array gain due to signal mismatch is related to  $G_w$  by [18]

$$S_w = \frac{1}{G_w} \quad (2.25)$$

Used in this context,  $S_w$  or  $G_w$  is a measure of robustness. Using  $\mathbf{w}_{MVDP}$  calculated in equation 2.19 for a perfectly matched processor with  $\mathbf{S}_x = \mathbf{I}$ ,  $G_w$  equals  $N$  and the beamformer is robust. ( $\mathbf{w}_{MVDP}$  for this case is a normalized, uniform weighting.) Any deviation from  $N$  indicates a degradation in beamformer robustness.

One additional expression for the array gain which turns out to be useful relates  $G$  in terms of eigenvalues and eigenvectors of  $\mathbf{Q}$ . The expression is

$$G = \sum_{i=1}^N \frac{|\mathbf{d}^\dagger \mathbf{v}_i|^2}{\lambda_i} \quad (2.26)$$

where  $\lambda_i$  and  $\mathbf{v}_i$  are the eigenvalues and eigenvectors, respectively.[18] This expression shows that  $G$  is dominated by small ratios of  $|\mathbf{d}^\dagger \mathbf{v}_i|^2/\lambda_i$ . This effect is not well understood because when  $\lambda_i$  is small,  $\mathbf{d}^\dagger \mathbf{v}_i$  is usually small also.

### 2.2.5 Spatial Scanning

The remaining feature to be specified is the spatial scanning problem. The spatial field, as previously defined, is the half space in which the array is located. To fully define the directional spectrum, the spatial field must be scanned or sampled. Equation 2.14 defines the method yet does not answer the question, "how finely must this field be sampled?" The spatial sampling interval is defined in terms of Nyquist's sampling requirements. This requires sampling at one half the natural beam width of the array which is equivalent to sampling at twice the highest frequency of the field or spatially at  $\lambda/2$ . Three factors must be considered when determining the sampling requirements.

1. As described in reference [19], finer sampling results in a visual display with significantly more content. This additional content is valuable when evaluating hard copy or video outputs of the directional spectrum.

2. If the natural beam width is determined by assuming the array is approximately rectangular, then error will be introduced into the values obtained.
3. The MVDP beamformer is susceptible to serious signal suppression effects due to signals arriving from directions between the processor beams. Minimizing this effect requires more closely spaced scan directions.[17]

Consideration of these three factors leads to the selection of a scanning increment of  $1/4$  the natural beam width ( $BW$ ). Verifying this is the proper decision requires the evaluation of  $1/2$  and  $1/8$   $BW$  scanning increments. There is one additional consideration when determining the proper scanning increment; it involves the computational burden. To illustrate this, the natural beam width of the array must be determined.

For the test array,  $BW$  is resolved into two directions called elevation (also known as depression/elevation or D/E) and azimuth. These directions arise naturally when anticipating an operational scenario; elevation is an angular measure off of a horizontal plane (+90 degrees to -90 degrees) and azimuth is an angular measure fore and aft of a vertical plane through the center of the array (0 degrees forward to 180 degrees aft). To determine  $BW$  the assumption that the array is approximately uniform and rectangular is applied.  $BW$  for a uniform rectangular array in the  $x$  direction is [20]

$$BW_x = \frac{\lambda}{L_x} \quad (2.27)$$

For the azimuthal direction,  $L_{azimuth} = 4.75\lambda$  and

$$BW_{azimuth} = 0.067\pi \approx 12^\circ \quad (2.28)$$

This leads to a azimuthal scanning increment of 3 degrees. In elevation (where the rectangular array approximation is least valid),  $L_{elevation} = 2.15\lambda$  and

$$BW_{elevation} = 0.148\pi \approx 26\frac{2}{3}^\circ \quad (2.29)$$

This leads to a scanning increment in elevation of  $6\frac{2}{3}$  degrees.

The scanning increment is implemented using uniform angular separation. The scanning system is best described using a global coordinate system of latitude and longitude

scan pattern	$L_e$	$L_a$	$L$
1/8 BW	54	118	6372
1/4 BW	27	59	1593
1/2 BW	14	30	420

Table 2.1: Summary of Computational Requirements for Different Scan Patterns

where latitude corresponds to azimuth and longitude corresponds to elevation. The procedure implementing the spatial sampling is to choose  $L_a$  latitudes separated by the azimuthal scanning increment. Then along each latitude,  $L_e$  longitudes are chosen separated by the elevation scanning increment. The total number of scans,  $L$ , is

$$L = L_e L_a \quad (2.30)$$

Steers in azimuth (latitude) to  $0^\circ$  and  $180^\circ$  are independent of the elevation angle. To eliminate duplicate scans and place a scanning direction at  $90^\circ$  azimuth, a  $3^\circ$  offset is incorporated at  $0^\circ$  and  $180^\circ$  azimuth. This pattern results in  $L_a = 59$ . To place a scanning direction at  $0^\circ$ , a  $3\frac{1}{3}^\circ$  offset is incorporated at  $+90^\circ$  and  $-90^\circ$  elevation; this results in  $L_e = 27$ . Therefore, the total number of scans is  $L = 1593$ . The scanning pattern as projected onto a plane surface is shown in figure 2-6.

Now consider the computational requirements of this scanning pattern. To define the directional spectrum equation 2.21 must be calculated  $L$  times, once for each scan direction. For an  $N$  element array, equation 2.21 represents an  $N$  by  $N$  system of equations. Solving an  $N$  by  $N$  system of equations  $L$  times is a time intensive process. Likewise, to determine the beam pattern, equation 2.20 must be calculated  $L$  times. Fortunately, the  $N$  by  $N$  system of equations only needs to be solved once for the array steer direction. Table 2.1 lists the scanning requirements for 1/8 BW, 1/4 BW and 1/2 BW scanning patterns. Based on these computational requirements the desire is to sample the spatial field at the fewest number of points consistent with adequate beamformer performance.

The scanning pattern used is not ideal. The algorithm implementing this pattern is very simple; with simple modifications 1/2 BW and 1/8 BW scanning patterns can be tested. However, the use of uniform angular scanning as implemented does not translate

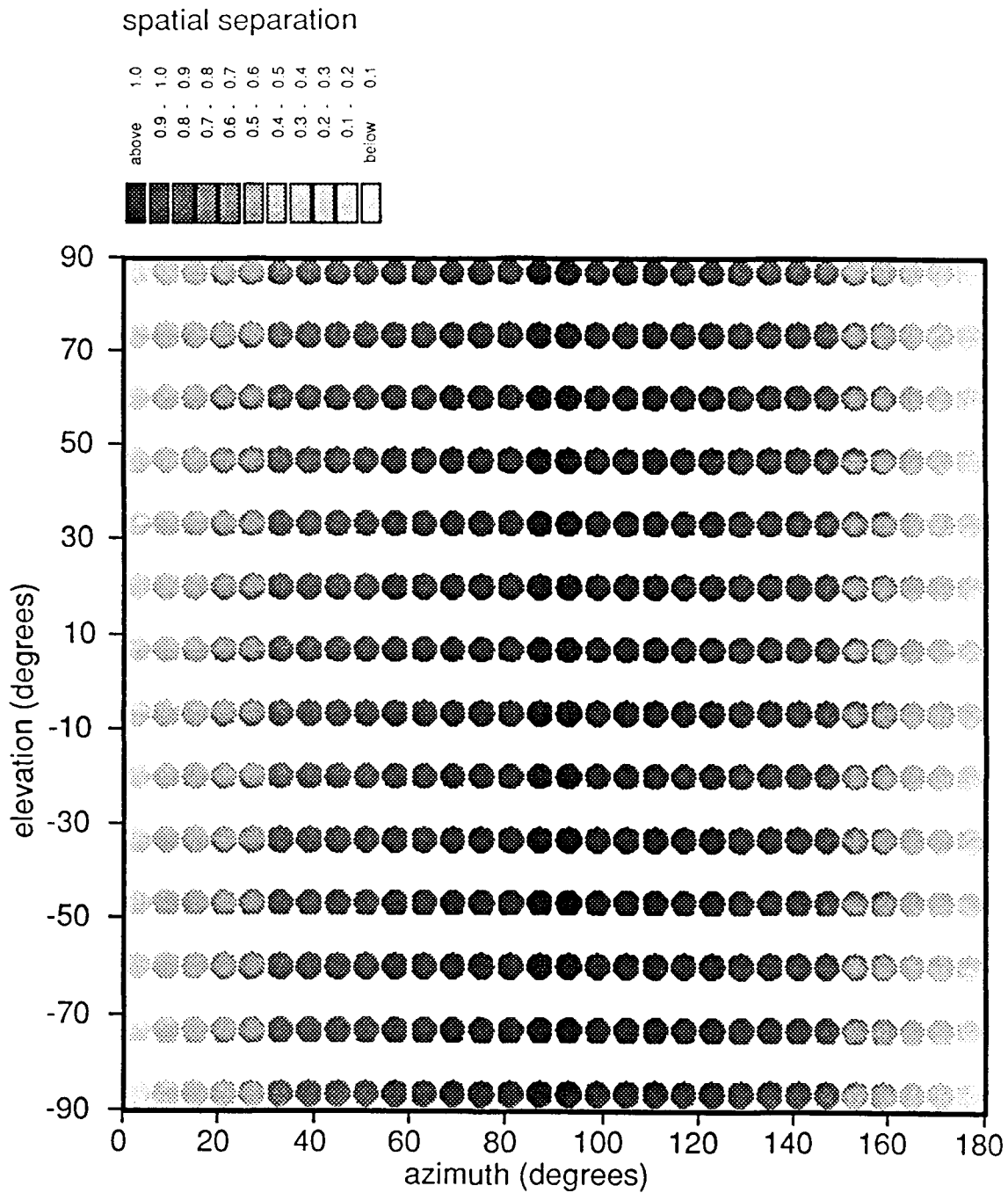


Figure 2-6: Projected Scanning Vector Locations. Every other scanning increment in elevation and azimuth is shown. The shading illustrates the variability in azimuth of the spatial separation between scan directions relative to the spatial separation at broadside resulting from the uniform angular scanning implementation.

into uniform spatial scanning. Whereas the spatial scanning is uniform in azimuth, the scanning in elevation is not spatially uniform, particularly in regions close to  $0^\circ$  and  $180^\circ$  in azimuth where the sampling in elevation is very dense. Figure 2-6 illustrates the differences in spatial scanning increment in elevation relative to the broadside spatial scanning increment. If this method of scanning is to be practically implemented, the optimum way is to rotate the pattern  $90^\circ$  and limit the elevation scanning region to the prime elevation angles of  $\pm 60^\circ$  where no structural shading occurs. This results in fairly uniform spatial scanning, but over a limited spatial region.

In summarizing the spatial scanning problem, a simple method that suits the purposes of the idealized synthetic investigation of the test array is presented. The scanning pattern occurs in uniform angular increments of  $3^\circ$  with 59 steers in azimuth and  $6\frac{2}{3}^\circ$  with 27 steers in elevation for a total of 1593 steers. The spatial increment corresponds to  $1/4 BW$  scanning. The simple scanning method is easily modified to allow the use of different scanning increments, but does not provide uniform spatial sampling.

## 2.3 Beam Pattern Design Method

In attempting to design beam patterns, the objective is to reduce the sidelobe levels compared to sidelobe levels characteristic of traditional shading methods. The beam pattern design procedure is implemented by the use of a "penalty function," so named because the function penalizes beam pattern lobes in regions of high directional intensity while enhancing the lobes in regions of low directional intensity. To understand this function, the actual processes undertaken by the MVDP beamformer must be understood in a qualitative manner.

The MVDP beamformer designs optimum beam patterns by minimizing the energy in the beam subject to the constraint of unity gain in the scan direction. The beam energy is represented as

$$S(f|\mathbf{k}_T) = \int P(f, \mathbf{k}) |\mathcal{W}|^2 d\mathbf{k} \quad (2.31)$$

which is interpreted as the integral over all wavenumber space of the frequency wavenumber function weighted by the square magnitude of the array response pattern (or beam

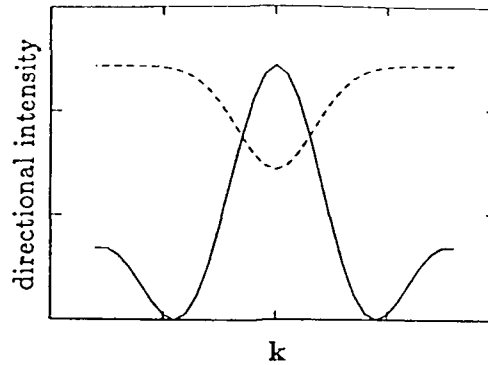


Figure 2-7: Null Placement Effects. For a source (solid line) incident at some  $k$ , the MVDP beamformer optimally places a null in the array response pattern (dashed line) in the direction of the source incident at  $k$ .

pattern). The MVDP beamformer designs array response patterns based on the frequency wavenumber function of the incident field in order to minimize the beam energy. If a discrete source not propagating in the look direction is incident (resulting in large  $P(f, k)$  for that direction), then  $|\mathcal{W}|^2$  is reduced to minimize the beam energy. The MVDP beamformer optimally places nulls in the directions of off-look direction sources.[15] This null placement effect is illustrated in figure 2-7. If diffused directional sources are located in a finite sector, then a lower array response occurs in the direction of the sector. However, the placement of deep nulls results in higher overall sidelobe levels which increases the effects of sensor noise, the other source term which contributes to total beam energy. Conversely, minimizing the effects of sensor noise by lowering overall sidelobe levels reduces the effects of nulls and increases the beam energy from off-look direction sources. The effects due to discrete directional sources and sensor noise are compromised until the minimum beam energy is obtained.

Since the desired effect is a reduction in sidelobe levels, the primary component of the penalty function consists of a field of diffuse directional sources of varying intensity. The field of directional sources is modeled similarly to isotropic noise which is directional noise incident uniformly from all directions with uniform intensity. The penalty function directional source component consists of a modified isotropic noise field, incident uniformly from all directions but with nonuniform intensity. In terms of equation 2.31, the penalty function (defined by  $P(f, k)$ ) in the directions of beam pattern sidelobes has high intensity

while in the direction of the beam pattern main lobe, has low intensity relative to the high intensity region. A three dimensional mesh representation of the penalty function is shown in figure 2-8. In regions of high intensity,  $|\mathcal{W}|^2$  is reduced. In regions of low intensity,  $|\mathcal{W}|^2$  can be large because the weighted integrated response is small. If the depressed sector of low intensity directional sources is centered about the steer direction and encompasses an area equivalent to the main beam region, the main beam of the resulting array response pattern will be large (supported by the unity gain constraint in the look direction) relative to the sidelobe region which is suppressed due to the uniformly distributed high intensity sources located in that region. The net effect is the desired result: a beam pattern with suppressed sidelobes. Figure 2-9 shows an overhead view of the penalty function centered about the steer direction. (The penalty function is always centered about the steer direction.) As shown, the penalty function consists of three regions.

1. The center region, defined by width in elevation ( $\Delta\theta_c$ ) and width in azimuth ( $\Delta\phi_c$ ), represents the low intensity region
2. The transition region, defined by width in elevation ( $\Delta\theta_t$ ) and width in azimuth ( $\Delta\phi_t$ ), serves as the interface between low and high intensity regions
3. The surrounding background region of high intensity

The issues pertinent to penalty function design are the shapes and widths of the center and transition regions, the amount of stabilization, and effects of the steer direction. Several of these parameters are discussed now; others are addressed in a later section.

The method used to input the penalty function into the array processor must take the form of a spectral covariance matrix. Using the same concepts as found in equations 2.8 and 2.11, the penalty function **PF** is defined as

$$\mathbf{PF} = \sigma_N^2 \mathbf{I} + \mathbf{S}_N \quad (2.32)$$

where  $\sigma_N^2$  is the sensor noise strength serving as a stabilization factor and  $\mathbf{S}_N$  is the directional component representing a modified isotropic noise field in terms of a sum of plane waves. The plane waves model this directional field at one half the scanning

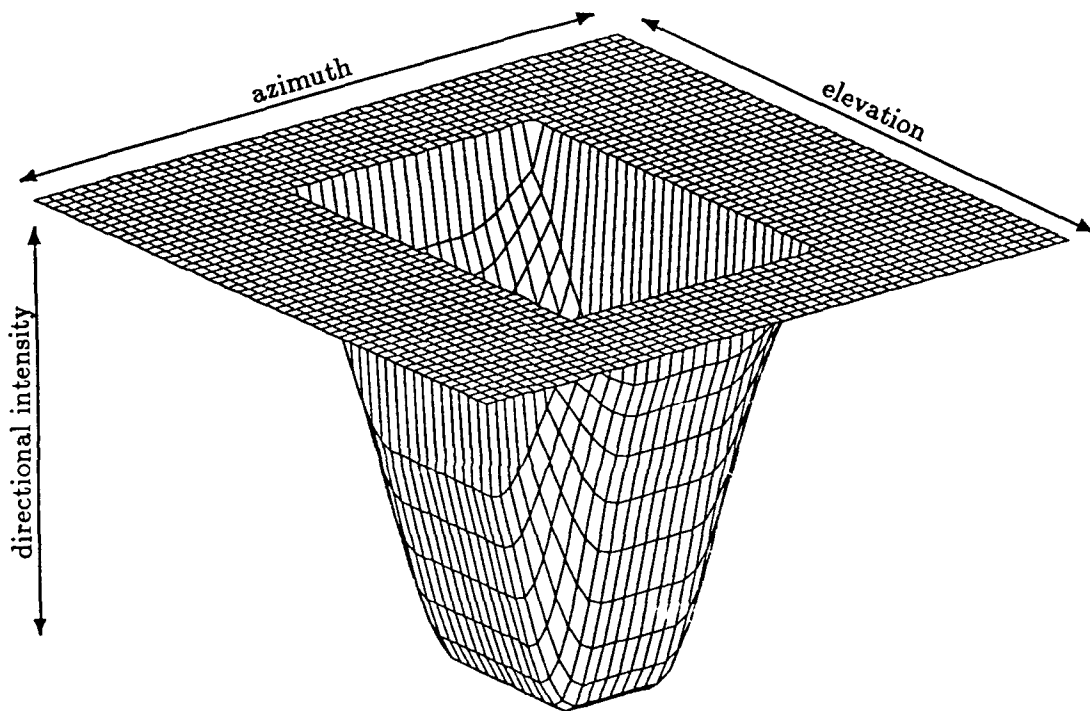


Figure 2-8: Three Dimensional Mesh Plot of Penalty Function

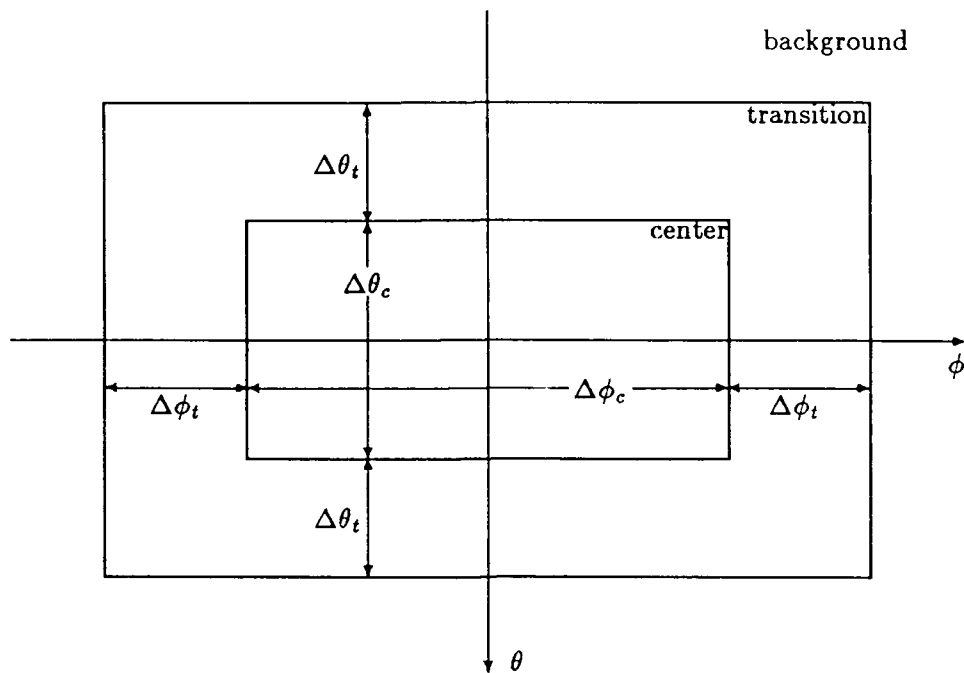


Figure 2-9: Overhead View of Penalty Function

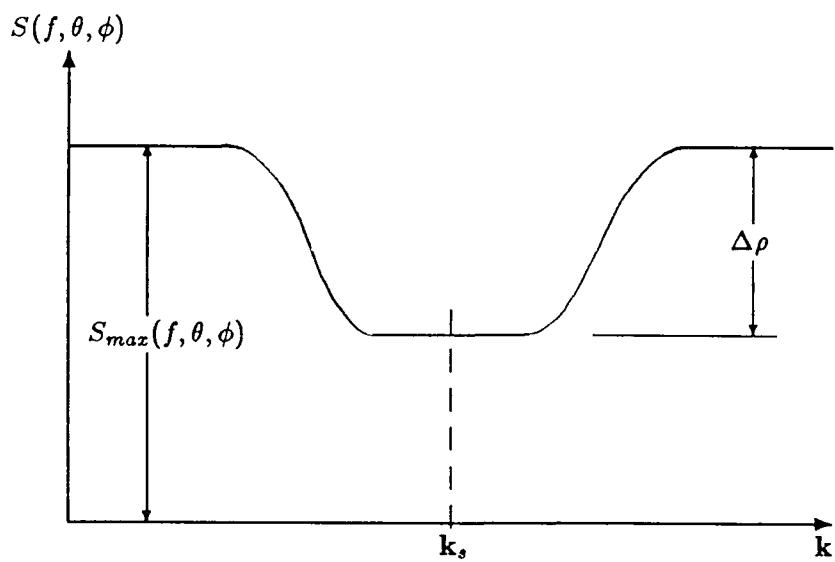


Figure 2-10: Two Dimensional Cross Section of Penalty Function

increment.  $S_N$  is defined as

$$S_N = \sum_{\phi=0}^{\pi} \sum_{\theta=0}^{\pi} S(f, \theta, \phi) \sum_{i=1}^{200} \sum_{j=1}^{200} e^{j \frac{2\pi}{\lambda} \mathbf{a}_r(\theta, \phi) \cdot \Delta \mathbf{z}} \quad (2.33)$$

where  $S(f, \theta, \phi)$  is a spatial weighting function acting on the plane waves and  $\mathbf{a}_r(\theta, \phi)$  is a unit directional vector defining the direction of propagation.  $\sum_{\phi=0}^{\pi} \sum_{\theta=0}^{\pi}$  represents the sum over the scanning space consisting of the half space in which the array is located.  $S_N$  is simply the sum of plane waves spatially weighted to form the distinct sectors shown in figure 2-9. A two dimensional cross section of  $S(f, \theta, \phi)$  is shown in figure 2-10. This illustrates the regions of high and low intensity. Two methods implementing the penalty function are now examined.

### 2.3.1 Method A

Method A uses the direct application of null placement to reduce beam pattern sidelobes. The high intensity directional noise field is formed with unit intensity while the low intensity region is formed with zero intensity (or no directional field). The sensor noise is then used to stabilize the process. The resulting directional noise field causes the sidelobes to be suppressed while the main lobe level is maintained by the unity gain constraint.

Referring to figure 2-10, method A is implemented by setting  $S_{max}(f, \theta, \phi) = 1$  and  $\Delta \rho = 1$ . In terms of equation 2.33, this requires

$$S_{A,center}(f, \theta, \phi) = 0 \quad (2.34)$$

$$S_{A,transition}(f, \theta, \phi) = \exp\left[-\frac{(\theta - \theta_o)^2}{2\sigma_\theta^2}\right] \exp\left[-\frac{(\phi - \phi_o)^2}{2\sigma_\phi^2}\right] \quad (2.35)$$

$$S_{A,background}(f, \theta, \phi) = 1 \quad (2.36)$$

This produces flat center and background regions interfaced by a Gaussian shaped transition region.  $\theta_o$  and  $\phi_o$  are the directions representing the appropriate center/transition region boundary. For a fixed number of increments in the transition region, the region dimensions and roll off's can be controlled by adjusting the variance ( $\sigma_\theta^2$  for elevation and  $\sigma_\phi^2$  for azimuth) of the Gaussian function.

### 2.3.2 Method B

Method B uses the opposite of null placement to reduce sidelobes. Instead of placing nulls in the sidelobe region, anti-nulls are placed in the main lobe region. This is accomplished by forming the high intensity region with zero intensity (no directional sources) while forming the low intensity region with negative intensity sources. The low intensity region still has lower intensity relative to the high intensity region. The effect of sidelobe suppression is indirectly accomplished with method B. The negative intensity (or low intensity) region can support very large main beam levels since the integrated beam energy from equation 2.31 is small. This effectively enhances the main lobe. The sidelobes are suppressed when the unity gain constraint scales the large main lobe. The sensor noise is again used to stabilize the process; however, greater stabilization is required for method B than is required for method A.

Referring to figure 2-10, method B is implemented by setting  $S_{max}(f, \theta, \phi) = 0$  and  $\Delta\rho = 1$ . In terms of equation 2.33, this requires

$$S_{B,center}(f, \theta, \phi) = -1 \quad (2.37)$$

$$S_{B,transition}(f, \theta, \phi) = -\exp\left[-\frac{(\theta - \theta_o)^2}{2\sigma_\theta^2}\right]\exp\left[-\frac{(\phi - \phi_o)^2}{2\sigma_\phi^2}\right] \quad (2.38)$$

$$S_{B,background}(f, \theta, \phi) = 0 \quad (2.39)$$

The region shapes and dimensions are controlled in the same manner as in method A.

In order to discuss the other issues, quantitative measures which enable an evaluation of those relevant issues must be determined. In particular, measures are needed to evaluate the effects of region widths and the amount of stabilization required.

## 2.4 Beamformer Performance Measures

### 2.4.1 Eigenvalues

Equation 2.21 requires that some specific restrictions be placed on the spectral covariance matrix of the penalty function. The most significant requirement is that  $S_x$  must be invertible. For a meaningful problem, this is ensured by requiring  $S_x$  be positive definite.

The approach taken to ensure this requirement is satisfied centers around the eigenvalues of  $S_x$ .

In section 2.2.2, it was determined that  $S_x$  is Hermitian which results in some special eigenvalue properties. All eigenvalues in this investigation are calculated using the Hermitian matrix routines available in the EISPACK eigensystem package.[21] Since eigenvalues of Hermitian systems are always real [22], a simple characterization of  $S_x$  is obtained. This simple characterization has physical interpretation which is now pursued.

Consider the eigenvalue problem

$$S_x \mathbf{v}_i = \lambda_i \mathbf{v}_i \quad (2.40)$$

where  $\lambda_i$  is the  $i^{\text{th}}$  eigenvalue and  $\mathbf{v}_i$  is the eigenvector corresponding to  $\lambda_i$ .  $S_x$  can be characterized as a measure of the energy of the received signals (similar to the eigenvalue interpretation of array gain.) This leads to an energy interpretation of eigenvalues where  $\lambda_i$  is a measure of the energy projected in the direction of  $\mathbf{v}_i$ . Small  $\lambda_i$  represent eigenvectors with low intensity. Low energy levels are associated with eigenvectors corresponding to the low intensity region of the penalty function. Again, this is consistent with the eigenvalue representation of array gain where small eigenvalues correspond to components with less noise.[17] Since  $S_x$  must be positive definite, the smallest eigenvalue,  $\lambda_{min}$ , must satisfy

$$\lambda_{min} > 0 \quad (2.41)$$

Intuitively, a penalty function with finite (and positive) energy throughout the scanning space as measured at the sensor is specified since negative or zero energy systems do not possess physical interpretations in the ocean environment.

With this interpretation for  $S_x$ , positive definite matrices can easily be generated. The value of  $\lambda_{min}$  is controlled by the stability factor. By generating a fixed coherent field by equation 2.33,  $\lambda_{min}$  is varied by adjusting  $\sigma_N^2$  in equation 2.32.

While the requirement of equation 2.41 is essential,  $\lambda_{min}$  must also be considered jointly with  $\lambda_{max}$ , the maximum eigenvalue. In particular, the ratio of  $\lambda_{max}/\lambda_{min}$  is very important. This ratio characterizes the dynamic range of  $S_x$ . A large dynamic range places more demands on the beamformer than a small dynamic range; therefore, dynamic range is an important issue when considering beamformer performance. Dynamic range

is applied in the area of array sensitivity and superdirectivity and is considered in the next section.

### 2.4.2 Sensitivity Ratio

The robustness constraint used in the investigation incorporates the principles associated with the white noise array gain.  $S_w$ , related to  $G_w$  by equation 2.25, is a measure of sensitivity to uncorrelated tolerance errors.[17] To ensure robust beamformer performance a constraint is applied to  $S_w$ . [18] The robustness constraint is applied to prevent superdirective performance. Superdirective performance is undesirable because a superdirective array is very sensitive to sensor noise and uncorrelated mismatch errors. Superdirectivity is characterized by extremely low values of  $G_w$ .

The actual constraint applied couples  $G_w$  to a parameter called the array sensitivity ratio  $\eta$  which is defined as

$$\eta = N\mathbf{w}^\dagger\mathbf{w} \quad (2.42)$$

Equation 2.42 is derived by substituting for  $\mathbf{w}_{MVDP}$  (as defined in equation 2.19) into equation 2.24. After some matrix manipulation (since  $\mathbf{S}_x$  is Hermitian, then  $\mathbf{S}_x^{-1}$  is also Hermitian), the result is

$$G_{w,MVDP} = \frac{|\mathbf{e}^\dagger\mathbf{S}_x^{-1}\mathbf{d}|^2}{\mathbf{e}^\dagger\mathbf{S}_x^{-2}\mathbf{e}} \quad (2.43)$$

Calculating  $\mathbf{w}^\dagger\mathbf{w}$  yields

$$\mathbf{w}^\dagger\mathbf{w} = \frac{\mathbf{e}^\dagger\mathbf{S}_x^{-2}\mathbf{e}}{(\mathbf{e}^\dagger\mathbf{S}_x^{-1}\mathbf{e})^2} \quad (2.44)$$

For the perfectly matched beamformer,

$$\mathbf{w}^\dagger\mathbf{w} = \frac{1}{G_{w,MVDP}} \quad (2.45)$$

Comparing to equation 2.25, it follows that the magnitude squared of the element weighting vector is a measure of beamformer sensitivity (or robustness.) Since  $G_w$  is always less than or equal to  $N$ , equation 2.42 is the ratio of the uniformly weighted  $G_w$  to  $G_{w,MVDP}$  or simply a measure of how far the MVDP beamformer white noise gain deviates from  $N$ . If  $\mathbf{w}$  represents a uniformly weighted aperture, then  $\eta$  equals 1 and the beamformer is robust. As the beamformer becomes less robust,  $\eta$  increases and the array becomes more sensitive.

The sensitivity ratio as defined in equation 2.42 is a very convenient measure of beam-former sensitivity since  $\mathbf{w}$  is available. But  $\eta$  must be related to superdirective array performance. Experience shows that superdirectivity occurs at sensitivity ratios in the range of 2.5 to 3.0; this leads to the constraint

$$\eta < 2.5 \quad (2.46)$$

The value of  $\eta$  is controlled by varying the dynamic range of  $\mathbf{S}_x$ . The addition of  $\sigma_N^2$  to the diagonal elements of  $\mathbf{S}_x$  adds  $\sigma_N^2$  to each eigenvalue and does not alter the eigenvectors.[18] Therefore, the inherent structure of the spectral covariance matrix is not changed. If  $\lambda_{min} \ll 1$ , then adjusting  $\lambda_{min}$  does not significantly affect  $\lambda_{max}$  thus controlling the dynamic range. Large dynamic ranges lead to superdirective array performance; therefore,  $\eta$  is controlled by limiting the dynamic range of  $\mathbf{S}_x$ .

### 2.4.3 Directivity Index

Until this point, the analysis of the array performance has been limited to an ideal ocean; one that has a perfectly coherent signal in incoherent noise. To examine the effects in a more realistic ocean environment, the requirement of incoherent noise is relaxed and the case of isotropic noise is considered.

Directivity index is defined as the array gain of a perfectly coherent signal in isotropic noise. Array gain can also be defined as the ratio, in decibel units, of the signal to noise ratio of an array to the signal to noise ratio of a single element. The directivity index is obtained by assuming a perfectly coherent signal which has cross correlation coefficients between pairs of array elements of

$$(\rho_s)_{i,j} = 1 \quad \forall i, j \quad (2.47)$$

and isotropic noise with cross correlation coefficients

$$(\rho_n)_{i,j} = \frac{\sin(\frac{2\pi}{\lambda}|\mathbf{z}_i - \mathbf{z}_j|)}{\frac{2\pi}{\lambda}|\mathbf{z}_i - \mathbf{z}_j|} \quad (2.48)$$

where  $\mathbf{z}_i$  is, as before, the position of the  $i^{th}$  element. Isotropic noise is defined as having the noise power per unit solid angle constant in all directions. Reference [1] describes it as

the superposition of plane waves propagating from all directions with uniform statistical level. Isotropic noise is commonly proposed as a first order model for ambient sea noise. Under these assumptions, the directivity index ( $DI$ ) can be calculated by

$$DI = 10 \log \frac{\sum_i \sum_j w_i w_j (\rho_s)_{i,j}}{\sum_i \sum_j w_i w_j (\rho_n)_{i,j}} \quad (2.49)$$

where  $w_i$  is the weight of the  $i^{th}$  element.[23]  $DI$  for a uniform rectangular array with dimensions corresponding to the test array is approximately 18 dB.[20]

Use of  $DI$  is an attempt to obtain a performance measure based on a "more" realistic ocean than previously considered. Since "real" ocean noise is directional in both the horizontal and vertical and ocean multipaths cause reduced signal coherence, the use of  $DI$  has practical limitations. However,  $DI$  is commonly used and is useful as a more realistic measure of beamformer performance in the real ocean.

## Chapter 3

# Beamforming Results

### 3.1 Preliminaries

Three preliminary issues must be resolved before the analysis of beam pattern designs can proceed. To aid in beam pattern analysis, a visual output is necessary. The relevant outputs used in this study are contour plots of the spatially scanned output, the beam pattern and the square magnitude and phase of the element weights. The contour plots are generated from a uniform grid of points. For the array output and beam pattern contours, the grid is 27 by 59. For the element weight contours, the grid is 10 by 20. Since the element weights are complex, it is convenient to plot the square magnitude of the weights and a corrected phase. The square magnitude of the weights are scaled to a maximum value of 1 (or 0 dB). The corrected phase ( $\Phi_i$ ) of the  $i^{th}$  element has the effect of the propagation delay across the array removed. This is calculated by

$$\Phi_i = \phi_i - \frac{2\pi}{\lambda} \mathbf{a}_r \cdot \mathbf{z}_i \quad (3.1)$$

where  $\phi_i$  is the element's actual phase,  $\mathbf{a}_r$  is the scan direction, and  $\mathbf{z}_i$  is the element's position vector. All four plots have axes corresponding to the angular position in the spatially scanned half space. For the magnitude and phase plots, these axes relate the element positions in terms of their location in the scanning field.

The next issue is the verification of the beamforming algorithm. The test used to verify proper operation is a plane wave incident at  $0^\circ$  elevation and  $90^\circ$  azimuth (true

broadside case) in the presence of sensor noise only. For this test the expected results are a sensitivity ratio of 1 (i. e.  $G_{w,MVDP} = N = 200$ ) and a uniform weighting vector. The MVDP beamformer results are as expected with  $DI = 39.2$ . The array output for this plane wave case is shown in figure 3-1. Observe that the array output correctly detects the plane wave. Figure 3-1 is also useful in that it provides some insight into the azimuthal and elevational resolution of the array processor. The beam pattern resulting from the plane wave input is the conventional beam pattern steered to  $0^\circ$  elevation and  $90^\circ$  azimuth; this is shown in figure 3-2. In figure 3-2, observe that there is unity gain in the scan direction as required in the MVDP derivation. Also, observe the first sidelobes (in both elevation and azimuth) are at -13 dB which is as expected for a uniformly weighted rectangular array. The second sidelobes in azimuth at -18 dB also correlate well with the rectangular array approximation. These two plots are useful as points of comparison for the broadside results. Results are also included for steered patterns, in particular, patterns steered to  $0^\circ$  elevation and  $102^\circ$  azimuth. For comparison purposes in anticipation of the steered results, the conventional beam pattern steered to  $0^\circ$  elevation and  $102^\circ$  azimuth is included in figure 3-3.

The last issue concerns the sufficiency of  $1/4 BW$  scanning. When a simple penalty function, set up to ensure directions between scanning increments are present, is input to the beamformer for the cases of  $1/8 BW$ ,  $1/4 BW$  and  $1/2 BW$  scanning, no observable effects due to incident plane waves between scan directions are present. Visually, the finer the scanning increment, the better (qualitatively) the output appears which is as expected. These results confirm the sufficiency of  $\frac{1}{4}BW$  scanning.

## 3.2 Broadside Results

The analysis of this investigation centers on a systematic evaluation of the effects of different penalty functions on beamformer performance (as measured by the sensitivity ratio and directivity index) and beam pattern structure. The parameters specifying the penalty function are listed in table 3.1 and are identified in chapter 2.3. The center region widths are easily defined; they are simply the widths of the plateau. The transition regio.

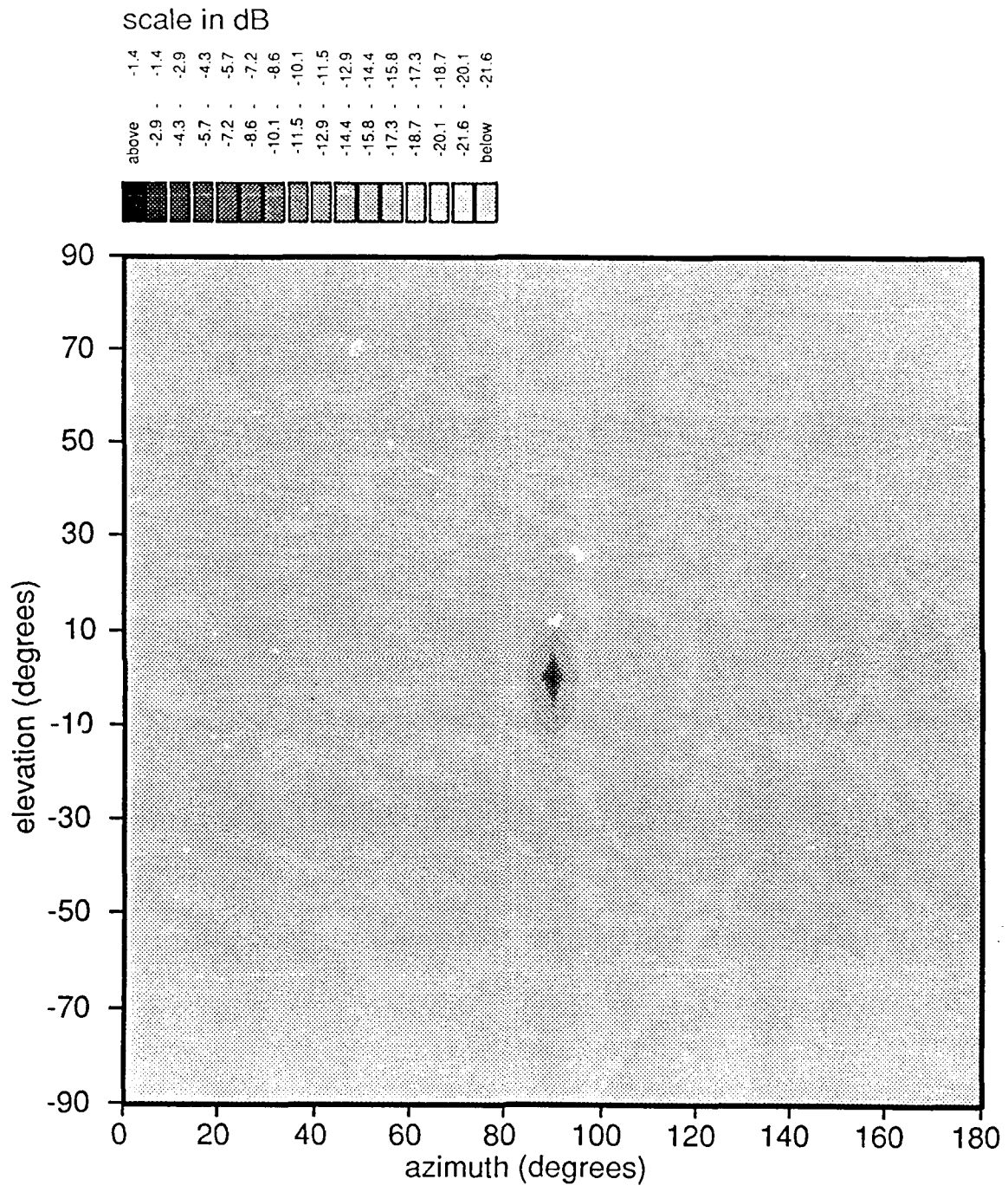


Figure 3-1: array output for plane wave case

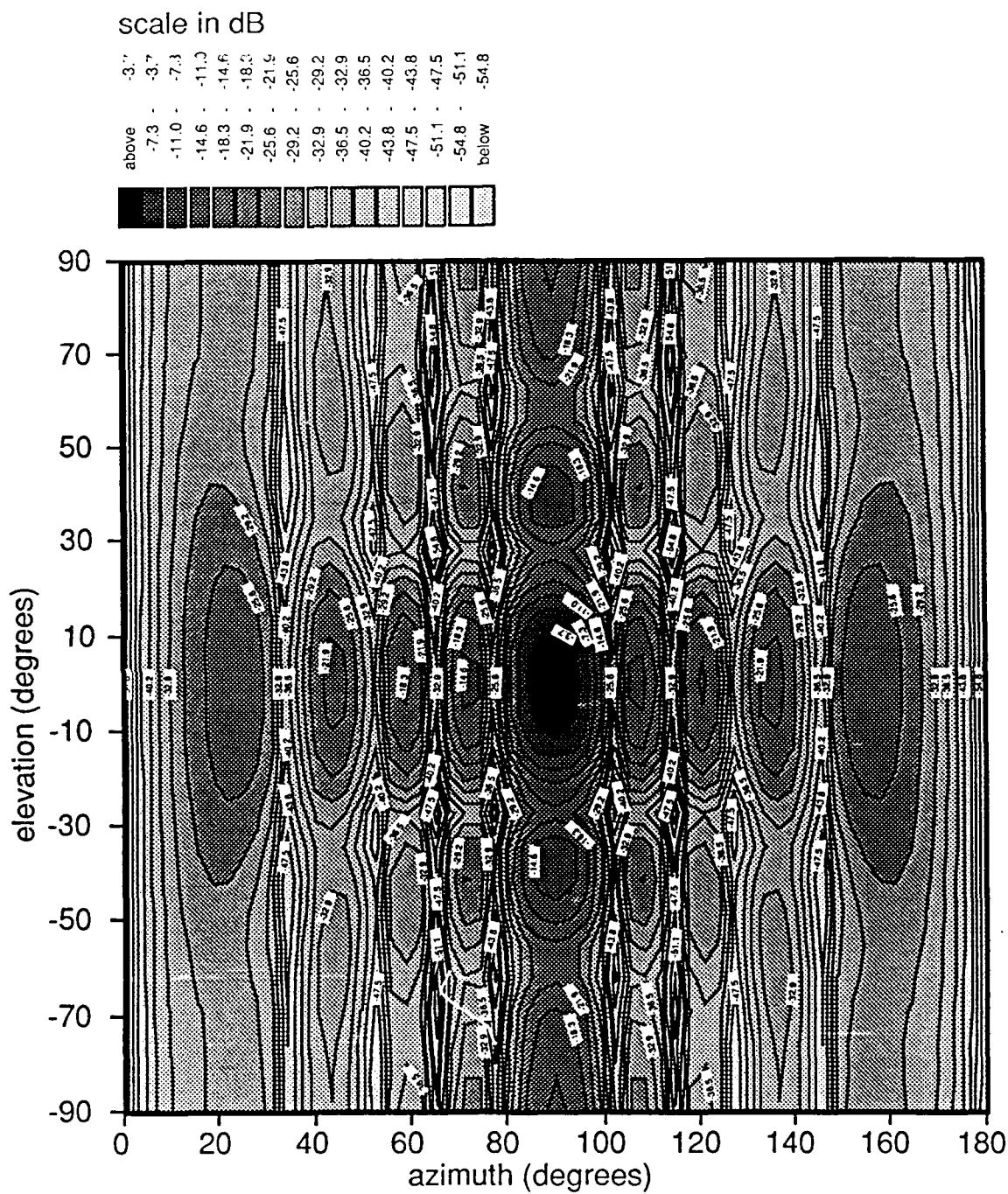


Figure 3-2: conventional beam pattern steered to 0° elevation and 90° azimuth

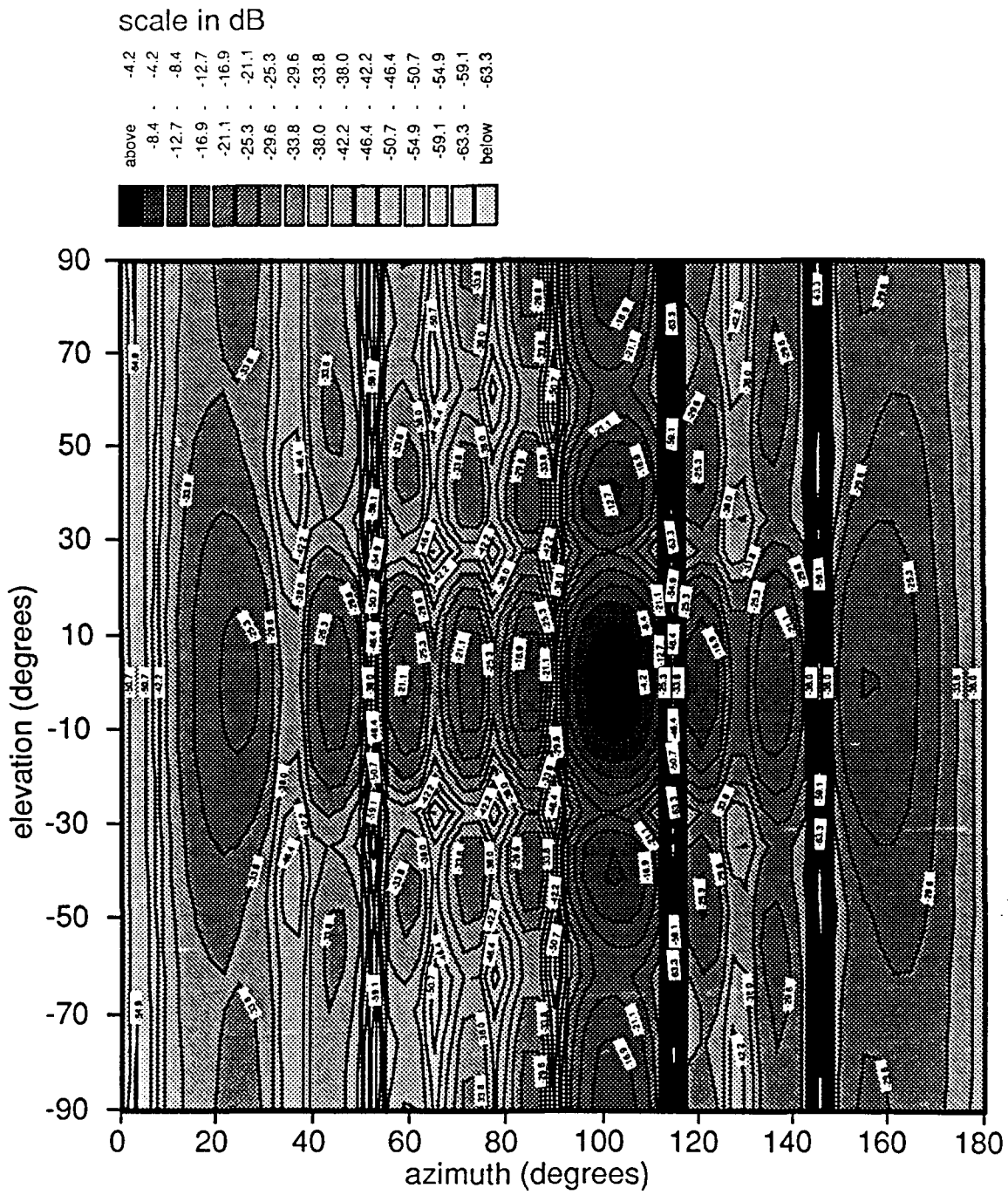


Figure 3-3: conventional beam pattern steered to 0° elevation and 102° azimuth

parameter	symbol	
minimum eigenvalue	$\lambda_{min}$	
center region width	elevation	$\Delta\theta_c$
	azimuth	$\Delta\phi_c$
transition region width	elevation	$\Delta\theta_t$
	azimuth	$\Delta\phi_t$

Table 3.1: Penalty Function Parameters

widths are more difficult to define. The widths are controlled by varying  $\sigma_\theta^2$  and  $\sigma_\phi^2$  in equation 2.38. From this,  $\Delta\theta_t$  and  $\Delta\phi_t$  are defined in terms of the 3 dB down points along the major axes. All region widths are measured in degrees. The investigation concentrates on penalty functions centered about  $0^\circ$  elevation and  $90^\circ$  azimuth; the bulk of the results come from the study of the broadside case. This scan direction is used for several reasons. First, patterns produced are symmetric and are very easy to analyze. A shift off of this scan direction produces very asymmetric patterns; these patterns are difficult to analyze. Second, this scan direction produces patterns that can be intuitively compared to a uniform rectangular array steered to broadside. Finally, it is easier to control the array output for method B penalty functions with the symmetric patterns. Since the two methods investigated have different behavior and characteristics, they will be addressed separately.

### 3.2.1 Method A

The first parameter to be resolved for both methods is the selection of  $\lambda_{min}$  or more specifically, the selection of the dynamic range of PF. From section 2.4.1, the larger  $\lambda_{min}$  can be correlated with larger values of  $\sigma_N^2$ . The more the  $\sigma_N^2$  term dominates in equation 2.32, the closer the penalty function resembles a sensor noise only case. This leads to the conventional beam pattern. Intuitively, the most interesting cases are for small  $\lambda_{min}$  or a large dynamic range. Experience gained from working with method A penalty functions shows that this method has very predictable performance with respect to dynamic range. For the penalty function parameters investigated with method A, the dynamic range which leads to a sensitivity ratio of approximately 2 is on the order of  $10^4$

minimum eigenvalue ( $\lambda_{min}$ )	dynamic range
$1 \cdot 10^{-3}$	$1.1 \cdot 10^4$
$2 \cdot 10^{-3}$	$5.6 \cdot 10^3$
$3 \cdot 10^{-3}$	$3.7 \cdot 10^3$
$5 \cdot 10^{-3}$	$2.2 \cdot 10^3$

Table 3.2: Minimum Eigenvalues and Associated Dynamic Ranges Tested for Method A Penalty Functions

with a corresponding  $\lambda_{min}$  on the order of  $10^{-3}$ . For purposes of comparison,  $\lambda_{min}$  for method A is restricted to the values listed in table 3.2.

With a dynamic range established, 15 cases are used to explore the effects of transition and center region widths on method A penalty functions. These 15 cases are summarized in table 3.3. Cases 1A through 5A examine the effects of center region width in azimuth. The best results in terms of  $DI$  and first sidelobe level occur with case 2A. For this case the first sidelobe level in azimuth is approximately -24.9 dB and in elevation is approximately -22.8 dB with  $DI = 37.9$  and  $\eta = 2.09$ . For all cases 1A through 5A, changing  $\Delta\phi_c$  has no effect on the first sidelobe level in elevation. Cases 6A through 11A examine the effects of center region width in elevation. Widths beyond  $52.5^\circ$  cause the first sidelobe to disappear. This results in wider main beam widths; therefore, cases beyond  $52.5^\circ$  are not considered. The best results occur with case 11A. The resulting first sidelobe level in azimuth is approximately -32.9 dB and in elevation is approximately -36.2 dB with  $DI = 37.4$  and  $\eta = 1.62$ . The eigenvalue performance characteristics for case 11A in terms of  $\eta$  and  $DI$  are shown in figure 3-4. As opposed to cases 1A through 5A, changing  $\Delta\theta_c$  significantly affects first sidelobe levels in azimuth where up to 8 dB differences are observed. This implies a partial coupling between azimuth and elevation first sidelobe levels. Using case 11A as the comparison point, cases 12A and 13A examine the effects of transition region width in azimuth while cases 14A and 15A examine the effects of transition region width in elevation. Transition region width appears to serve as a fine tuner in defining an effective method A penalty function width. The best results occur for case 11A; therefore, the array output, beam pattern, square magnitude and corrected phase for the elements weights are shown in figures 3-5 through 3-8. Figure 3-5 is the array

case	$\Delta\theta_c^\dagger$	$\Delta\phi_c^\dagger$	$\Delta\theta_t^\dagger$	$\Delta\phi_t^\dagger$
1A	15	15	16.2	16.2
2A	15	22.5	16.2	16.2
3A	15	30	16.2	16.2
4A	15	37.5	16.2	16.2
5A	15	45	16.2	16.2
6A	7.5	22.5	16.2	16.2
7A	22.5	22.5	16.2	16.2
8A	30	22.5	16.2	16.2
9A	37.5	22.5	16.2	16.2
10A	45	22.5	16.2	16.2
11A	52.5	22.5	16.2	16.2
12A	52.5	22.5	16.2	11.7
13A	52.5	22.5	16.2	21.0
14A	52.5	22.5	8.8	16.2
15A	52.5	22.5	28.6	16.2

<sup>†</sup>all widths in degrees

Table 3.3: Method A Case Study Summary

processor's representation of the penalty function. Figure 3-6 has significantly reduced sidelobes compared to the conventional beam pattern shown in figure 3-2. The weights, as defined in figures 3-7 and 3-8, do not possess a structure that is readily identified with a conventional weighting.

Based on the method A performance results, the penalty function design process for method A is summarized by the following rules:

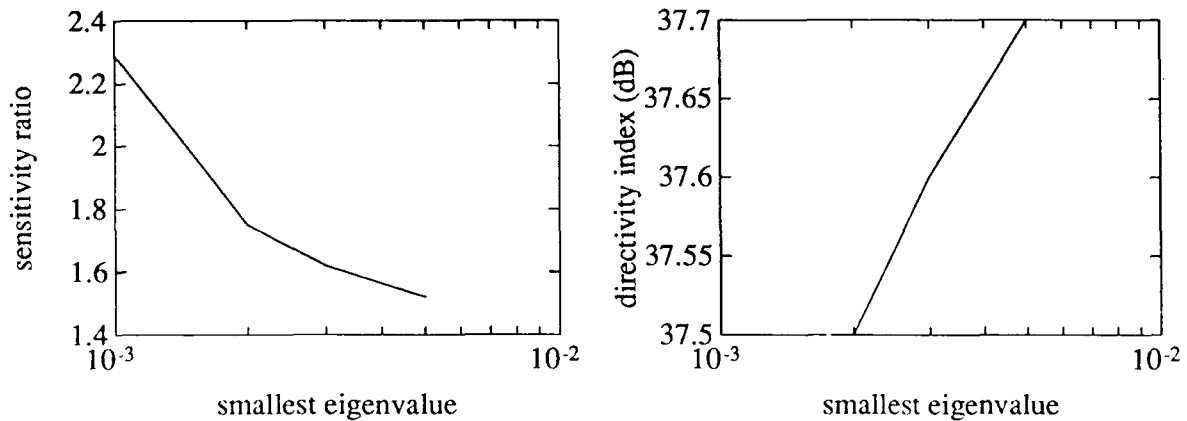


Figure 3-4: Eigenvalue Performance Results for Case 11A

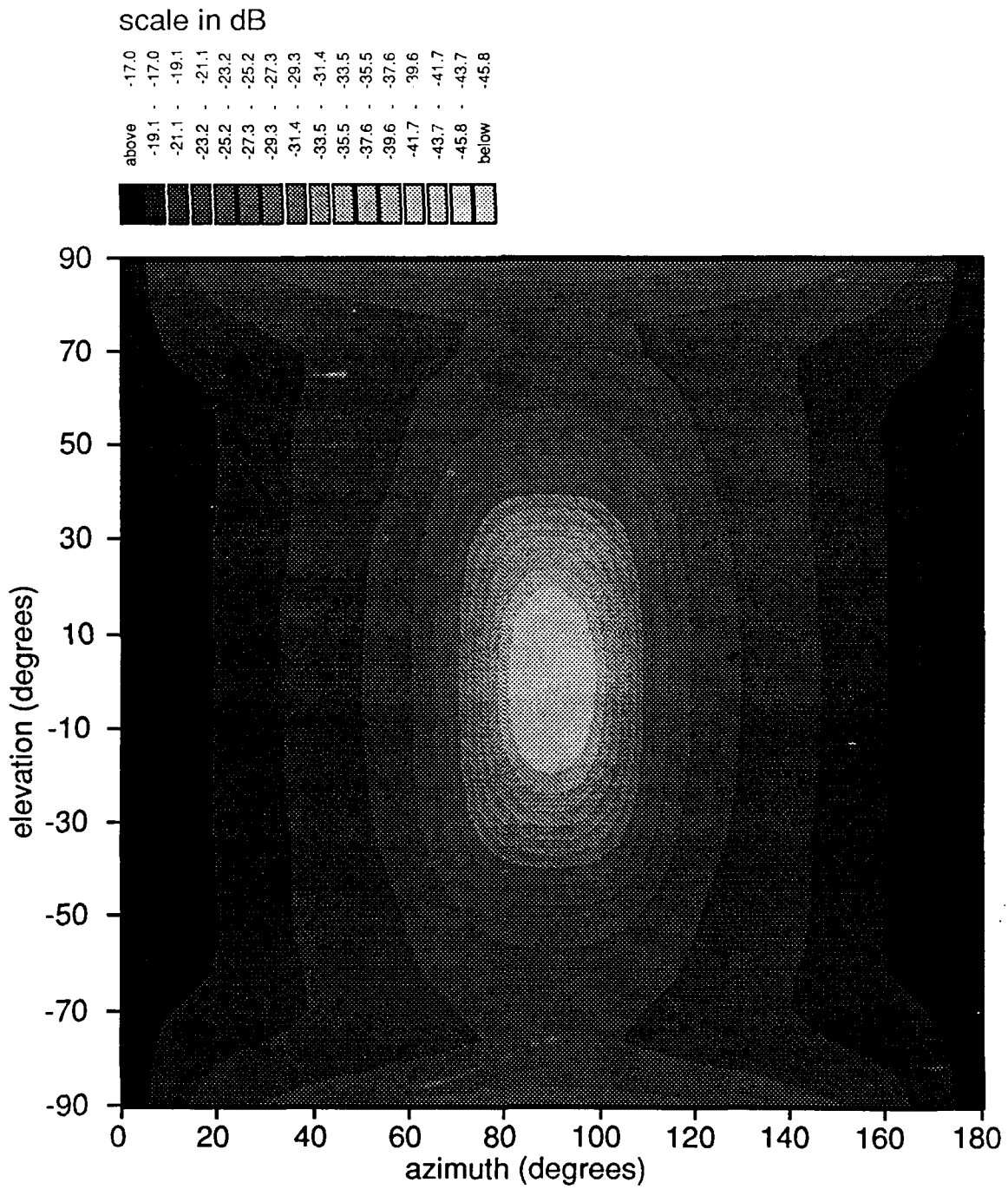


Figure 3-5: array output for case 11A,  $\lambda_{min} = 10^{-3}$

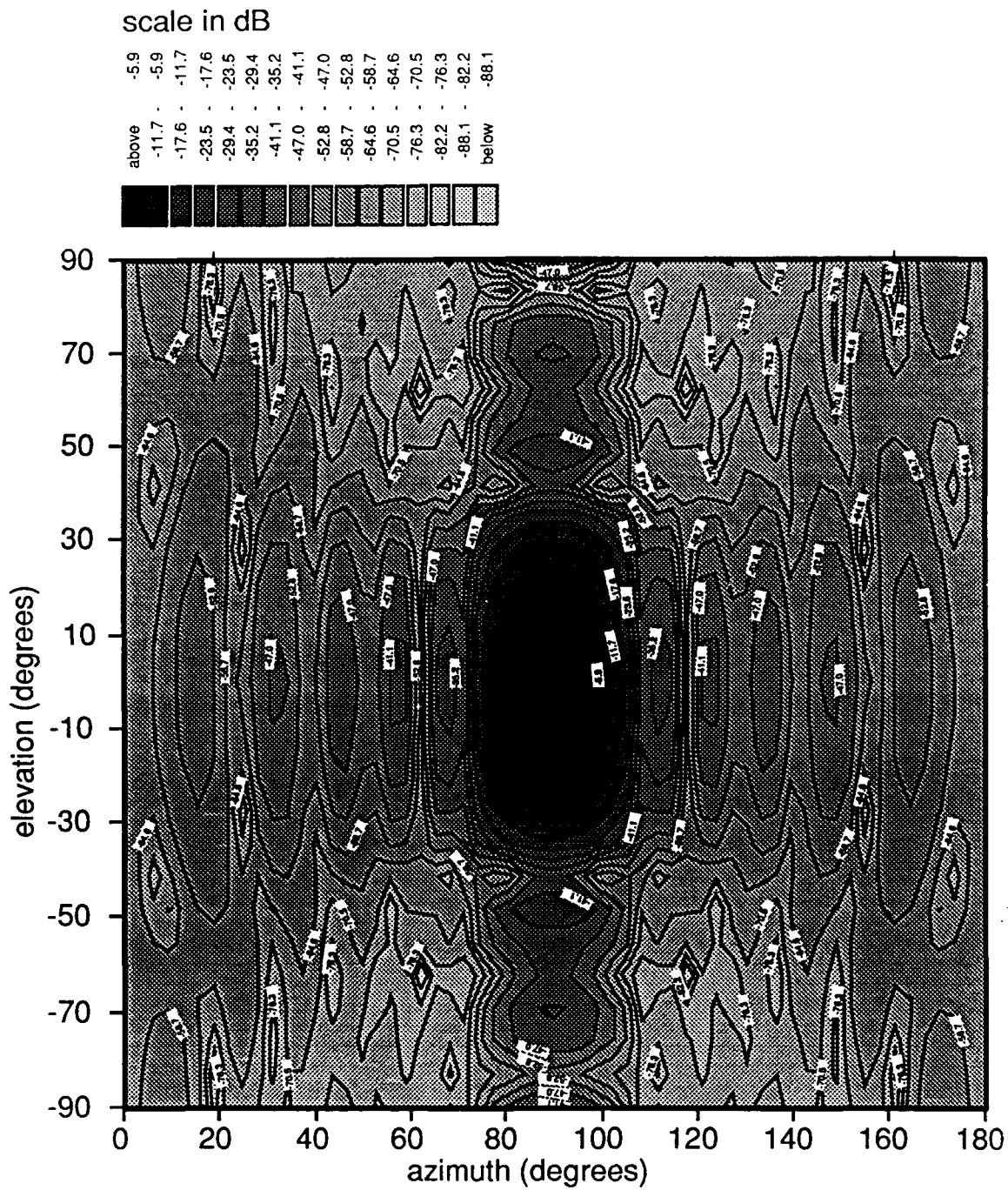


Figure 3-6: beam pattern for case 11A,  $\lambda_{min} = 10^{-3}$

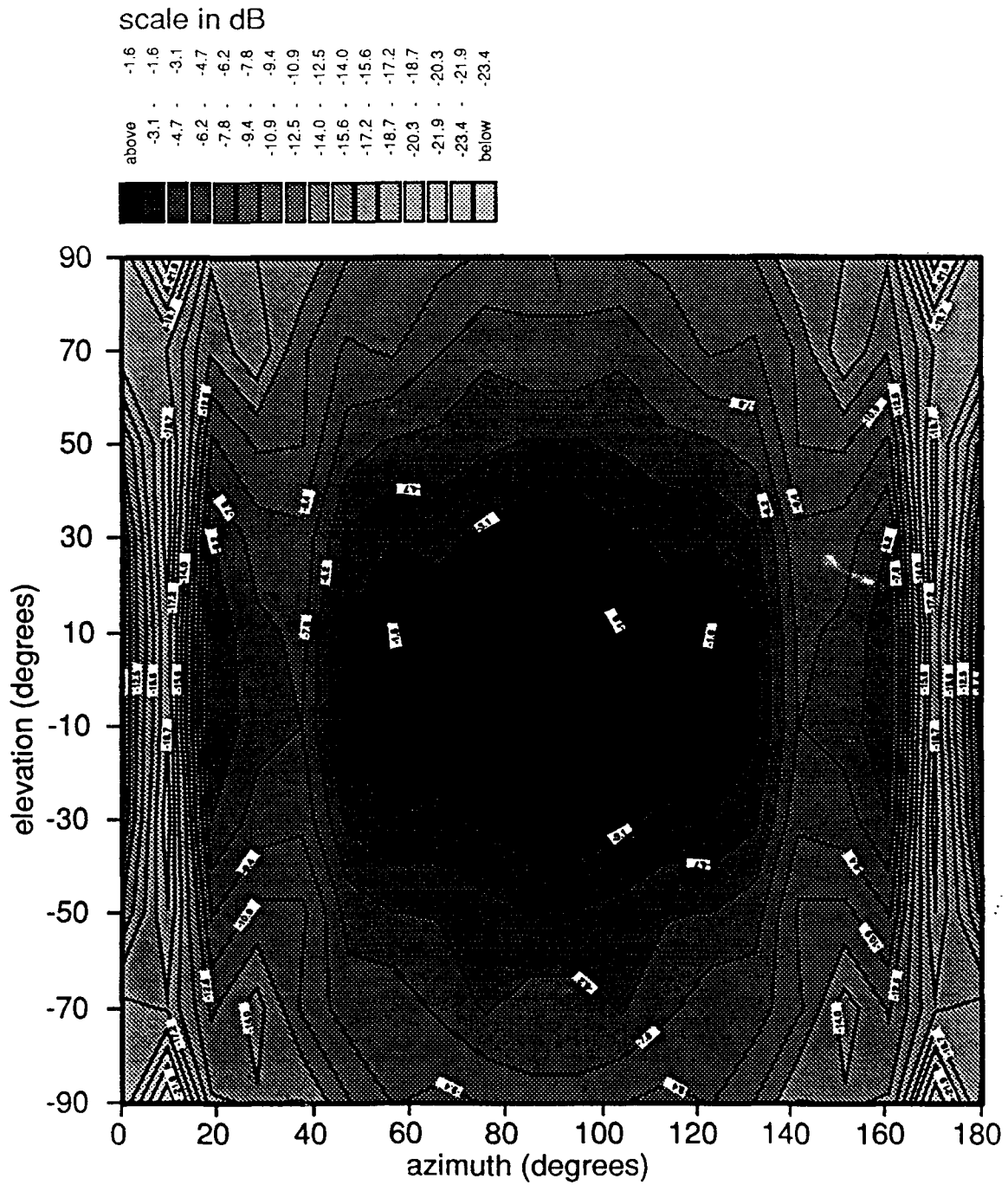


Figure 3-7: square magnitude of element weights, case 11A,  $\lambda_{min} = 10^{-3}$

scale in pi radians

above	0.792
0.663	- 0.792
0.535	- 0.663
0.406	- 0.535
0.277	- 0.406
0.148	- 0.277
0.019	- 0.148
-0.110	- 0.019
-0.238	- -0.110
-0.367	- -0.238
-0.496	- -0.367
-0.625	- -0.496
-0.754	- -0.625
-0.883	- -0.754
-1.011	- -0.883
below	-1.011

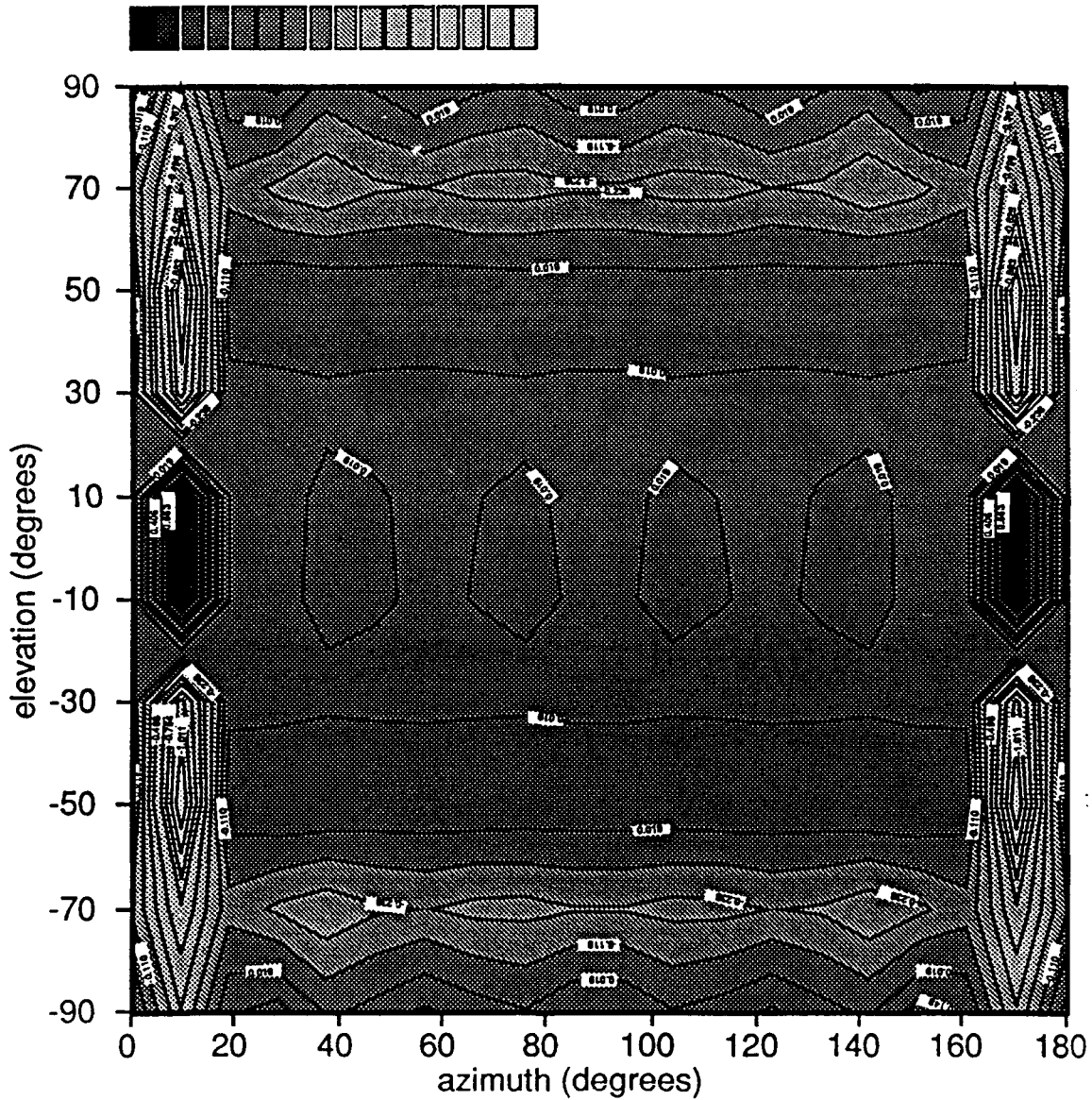


Figure 3-8: corrected phase of element weights, case 11A,  $\lambda_{min} = 10^{-3}$

- Selection of center region width is the most critical parameter choice and should be on the order of the width of the main beam of the conventional beam pattern.
- Center region widths in directions with a large aperture should be selected first since these widths appear to be uncoupled with directions with short apertures.
- The transition region widths should be selected to fine tune the effective penalty function width to yield a smooth transition over a region less than the width of the center region.
- Select a dynamic range that prevents superdirective performance. Large dynamic ranges (but still not superdirective) usually result in lower first sidelobe levels, wider main beams, and smaller  $DI$ , so some trade off may be desired in the selection of dynamic range.

Using these guidelines, a significant reduction in sidelobe levels can be achieved using the method A penalty function design process.

### 3.2.2 Method B

As was the case for method A, the dynamic range for method B penalty functions must first be established. This issue is not as easily addressed for method B as it is for method A. Although the most interesting cases are still for small  $\lambda_{min}$ , method B penalty functions exhibit unpredictable behavior in such a way that dynamic range must be considered as a separate issue for each case. Therefore to cover the majority of possibilities, the values of  $\lambda_{min}$  listed in table 3.4 are considered. These values of  $\lambda_{min}$  correspond to dynamic ranges varying from  $10^6$  to  $10^1$ .

The effects of transition and center region widths for method B penalty functions are explored in 13 cases which are summarized in table 3.5. Cases 4B and 5B have performance characteristics in terms of  $\eta$  and  $DI$  versus  $\lambda_{min}$  similar to method A; all are superdirective at large values of dynamic range. The remaining cases have different performance characteristics. These cases can not be driven superdirective even for very large dynamic ranges. In fact, these cases exhibit a stable performance region where no gain in sidelobe reduction is achieved with increasing dynamic range. The performance

minimum eigenvalue ( $\lambda_{min}$ )	dynamic range
$10^{-6}$	$9.5 \cdot 10^5$
$10^{-5}$	$9.5 \cdot 10^4$
$10^{-4}$	$9.5 \cdot 10^3$
$10^{-3}$	$9.5 \cdot 10^2$
$10^{-2}$	$9.5 \cdot 10^1$
$10^{-1}$	$9.5 \cdot 10^0$

Table 3.4: Minimum Eigenvalues and Associated Dynamic Ranges Tested for Method B Penalty Functions

results for case 9B (this case displays the best results of all 13 cases) are shown in figure 3-9. Observe the stable operating region for  $\lambda_{min} < 10^{-3}$ .

Cases 1B through 5B examine the effects of  $\Delta\phi_c$ . For cases 4B and 5B,  $\Delta\phi_c$  is too wide causing the first sidelobes to be emphasized in addition to the main lobe. This is the cause of the superdirective performance results. Case 3B results in the best sidelobe control with first sidelobe level in azimuth equal to -49.7 dB, first sidelobe level in elevation equal to -17.3 dB,  $\lambda_{min} = 10^{-4}$ ,  $\eta = 1.6$ , and  $DI = 34.6$  dB. No effects are observed on sidelobe levels in elevation for cases 1B through 5B.

Cases 6B through 8B examine the effects of  $\Delta\theta_c$ . All cases produce first sidelobe levels within 1 dB of each other, the best being case 7B with a first sidelobe level in elevation of -18 dB. Sidelobe levels in elevation are generally insensitive to method B penalty function parameter adjustment.

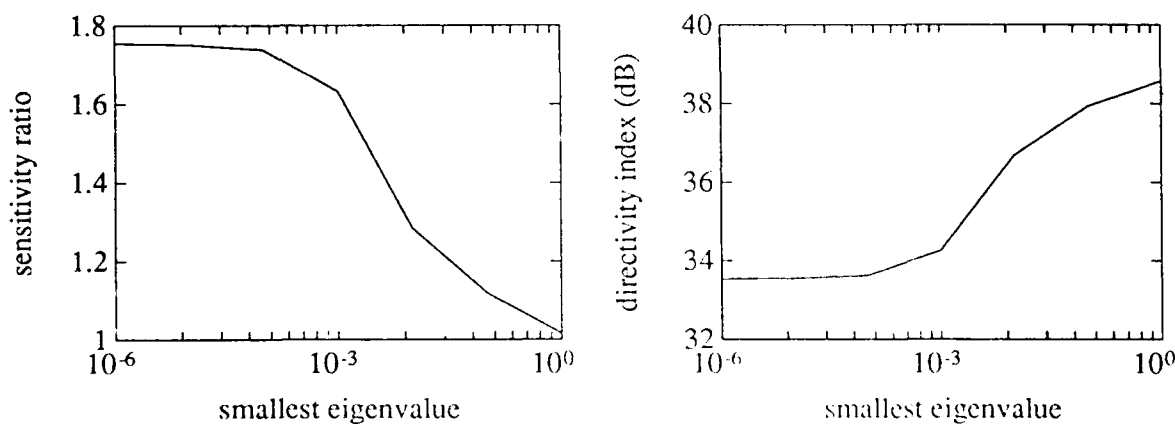


Figure 3-9: Eigenvalue Performance Results for Case 9B

case	$\Delta\theta_c^\dagger$	$\Delta\phi_c^\dagger$	$\Delta\theta_t^\dagger$	$\Delta\phi_t^\dagger$
1B	15	15	16.2	16.2
2B	15	22.5	16.2	16.2
3B	15	30	16.2	16.2
4B	15	37.5	16.2	16.2
5B	15	45	16.2	16.2
6B	7.5	22.5	16.2	16.2
7B	22.5	22.5	16.2	16.2
8B	30	22.5	16.2	16.2
9B	22.5	30	16.2	16.2
10B	22.5	30	16.2	11.7
11B	22.5	30	16.2	21.0
12B	22.5	30	8.8	16.2
13B	22.5	30	23.6	16.2

<sup>†</sup>all widths in degrees

Table 3.5: Method B Case Study Summary

Case 9B represents the best results of the center region width study and is used as the comparison case for the transition region width study. Cases 10B through 13B investigate the transition region width issue. Transition region effects for method B are similar to those effects for method A; transition region width serves as fine tuning for the effective penalty function width.

Case 9B represents the best results for all 15 cases. The array output, beam pattern, square magnitude and corrected phase of the element weights are shown in figures 3-10 through 3-13. Figure 3-10 shows the array processor's interpretation of the method B penalty function. The beam pattern in figure 3-11 has significantly reduced sidelobes in azimuth compared to the conventional beam pattern found in figure 3-2, but has only minor improvements in sidelobe levels in elevation. The element weights shown in figures 3-12 and 3-13 have a structure similar to conventional weights: high in the middle and tapering towards the ends.

The method B investigation also revealed several important issues characteristic of the method B penalty function. One, the beamformer tends to emphasize edges; in particular, the edges corresponding to the transition region. If the center region is wide enough, the

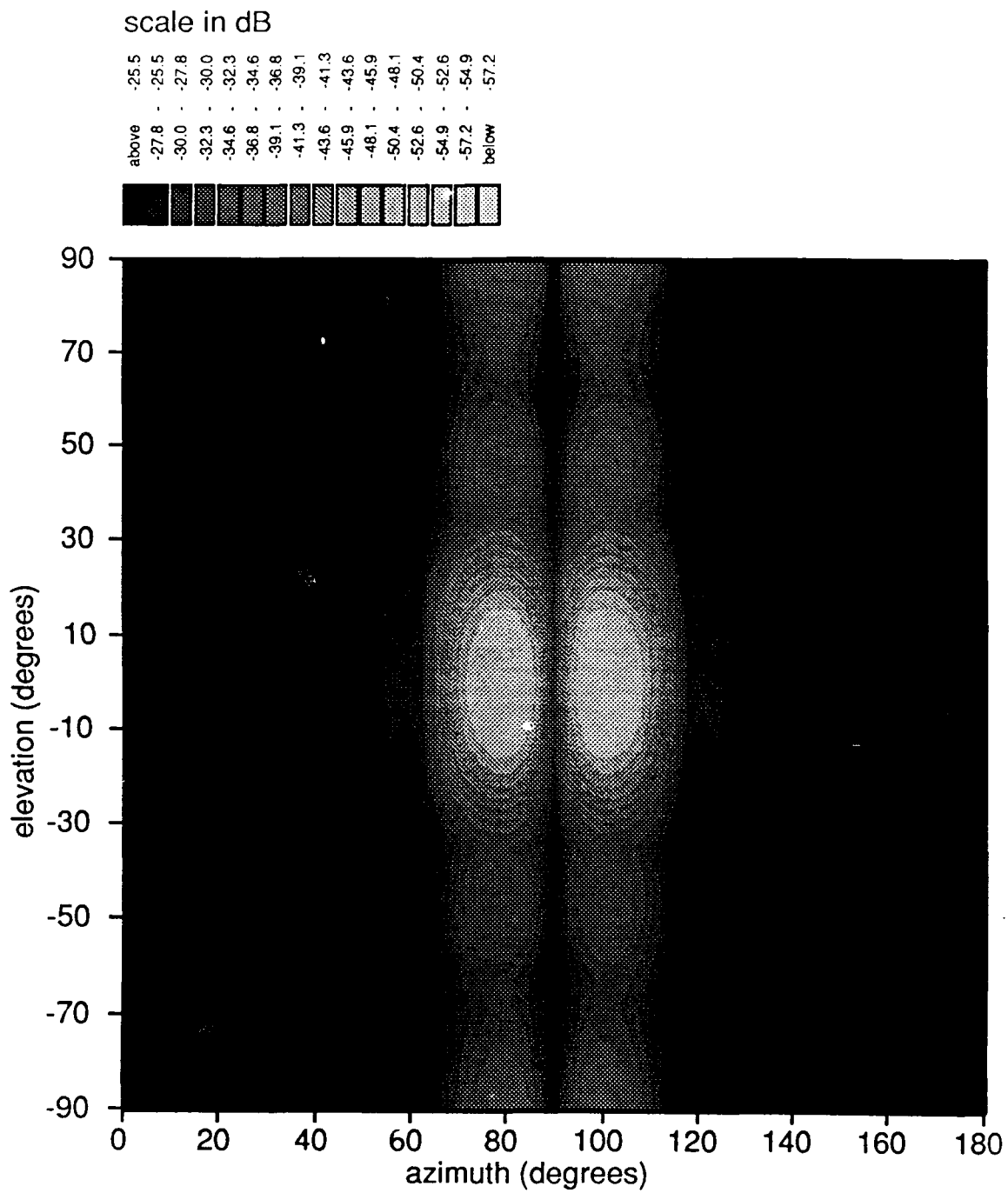


Figure 3-10: array output, case 9B,  $\lambda_{min} = 10^{-4}$

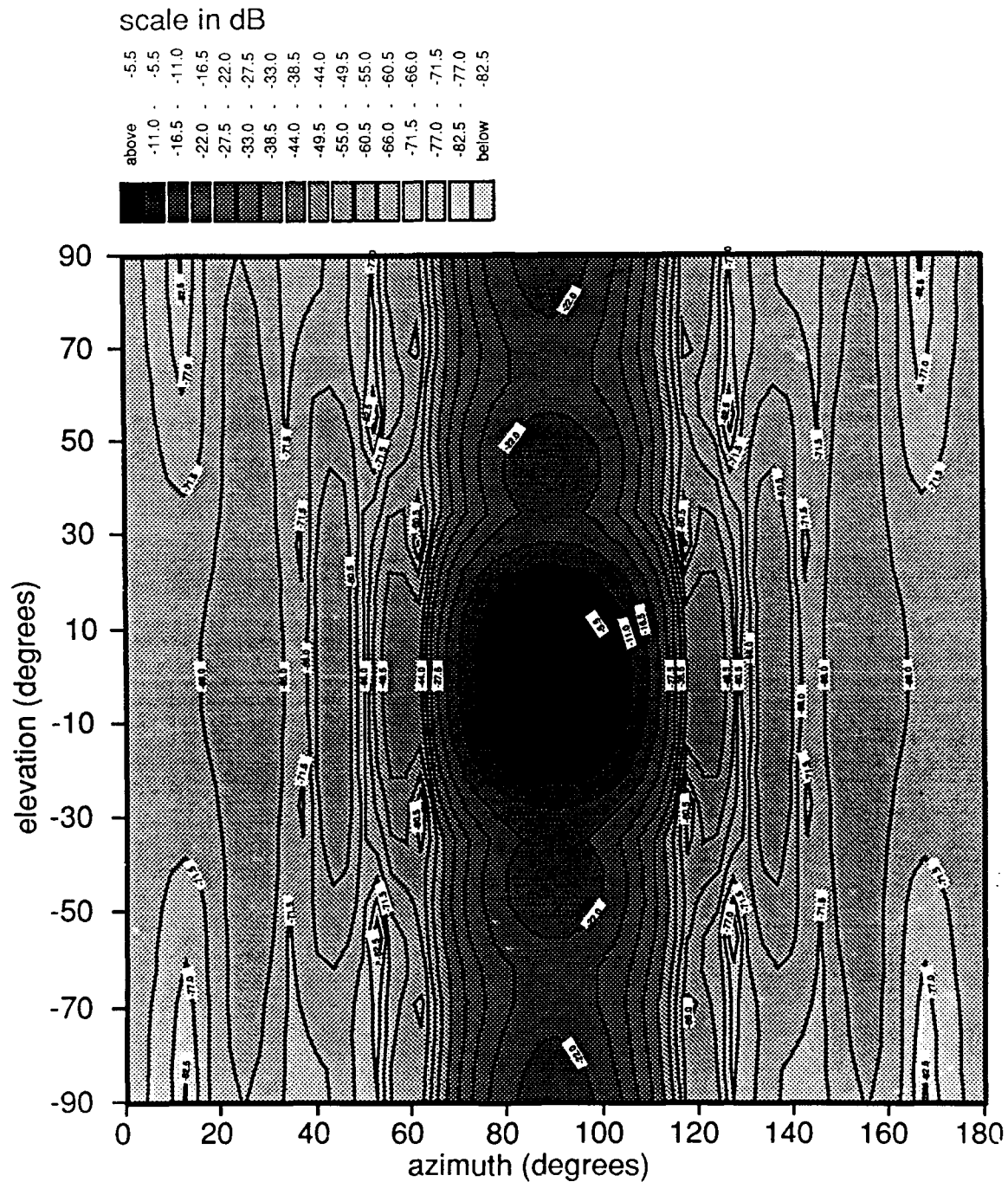


Figure 3-11: beam pattern, case 9B,  $\lambda_{min} = 10^{-4}$

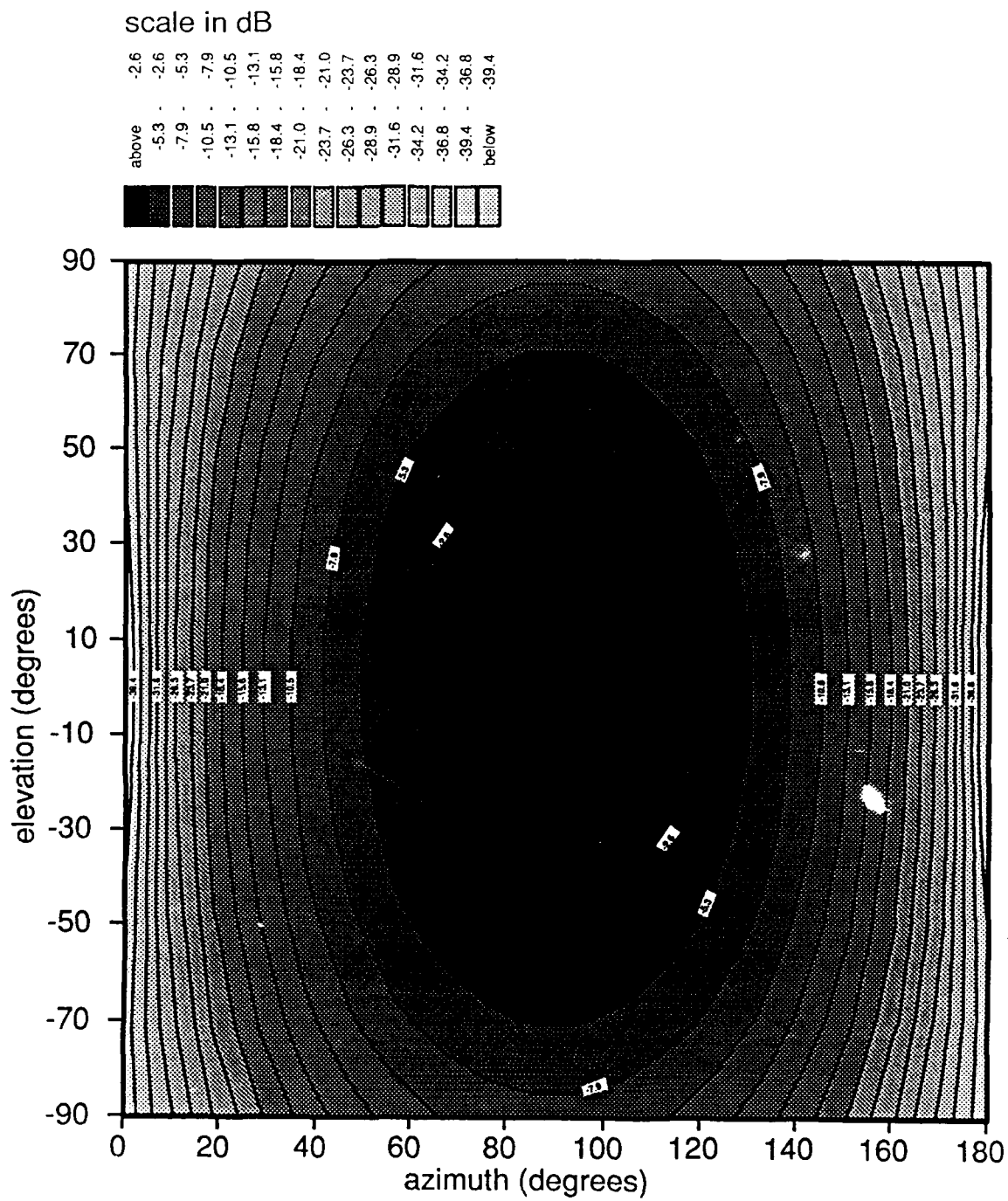


Figure 3-12: square magnitude of element weights, case 9B,  $\lambda_{min} = 10^{-4}$

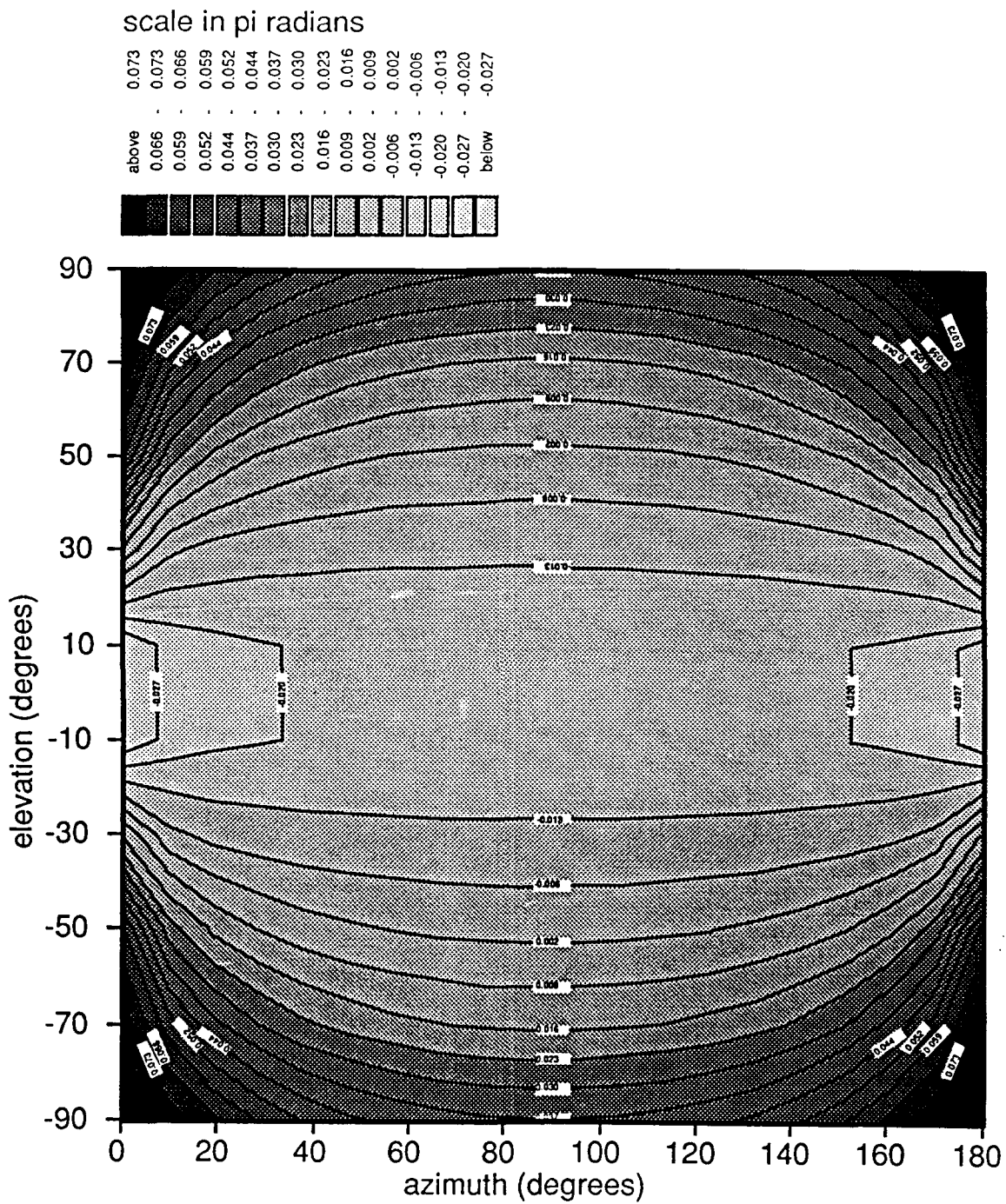


Figure 3-13: corrected phase of element weights, case 9B,  $\lambda_{min} = 10^{-4}$

edges are located in the vicinity of the first sidelobe of the conventional beam pattern. This is shown in figure 3-14, the case 5B array output. This results in the superdirective beam pattern found in figure 3-15. More significantly, the element weights appear to have a threshold where the structure changes suddenly to a significantly different shape. This is shown in figures 3-16 and 3-17.

The penalty function design process for method B is summarized by the following rules.

- Select a center region width on the order of the width of the main beam of the conventional beam pattern.
- Selection of the center region width involves a trade off against the array aperture. For those directions with large apertures (azimuth), the full main beam width should be used. For those directions with short apertures (elevation), the center region width must be limited to something less than the main beam width due to the wide main beam and low sensitivity to parameter adjustment.
- Select transition region widths to fine tune the effective penalty function width and to yield a smooth transition over a region less than the width of the center region.
- Select the smallest possible dynamic range that is located in a stable operating region if a stable region exists. Otherwise, choose the largest dynamic range consistent with superdirectivity and *DI* considerations.

Using these guidelines for method B designs, a significant reduction in levels can be achieved with the more notable results occurring in directions of large array aperture.

### 3.3 Steered Results

The problem encountered with steered penalty functions is the introduction of asymmetry into the problem. This asymmetry has very little effect on method A and has very significant effects on method B. Only limited results are presented here; a single case steered to  $0^\circ$  elevation and  $102^\circ$  azimuth is illustrated. The intent is to only provide an intuitive feel for steered penalty function performance.

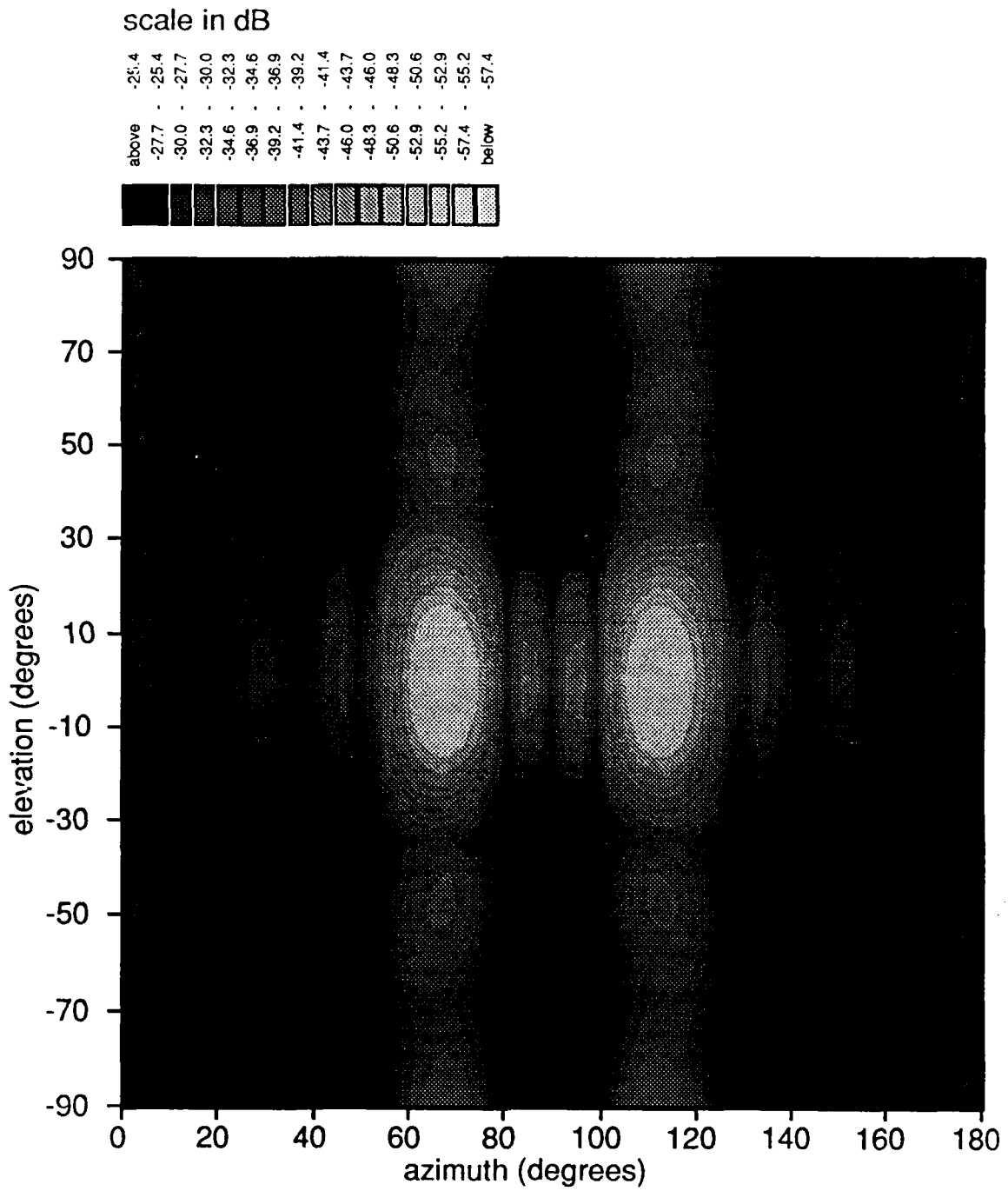


Figure 3-14: array output, case 5B,  $\lambda_{min} = 10^{-4}$

scale in dB

above	-4.7
-9.5	-4.7
-14.3	-9.5
-19.1	-14.3
-23.9	-19.1
-28.8	-23.9
-33.6	-28.8
-38.4	-33.6
-43.2	-38.4
-48.1	-43.2
-52.9	-48.1
-57.7	-52.9
-62.5	-57.7
-67.4	-62.5
-72.2	-67.4
below	-72.2

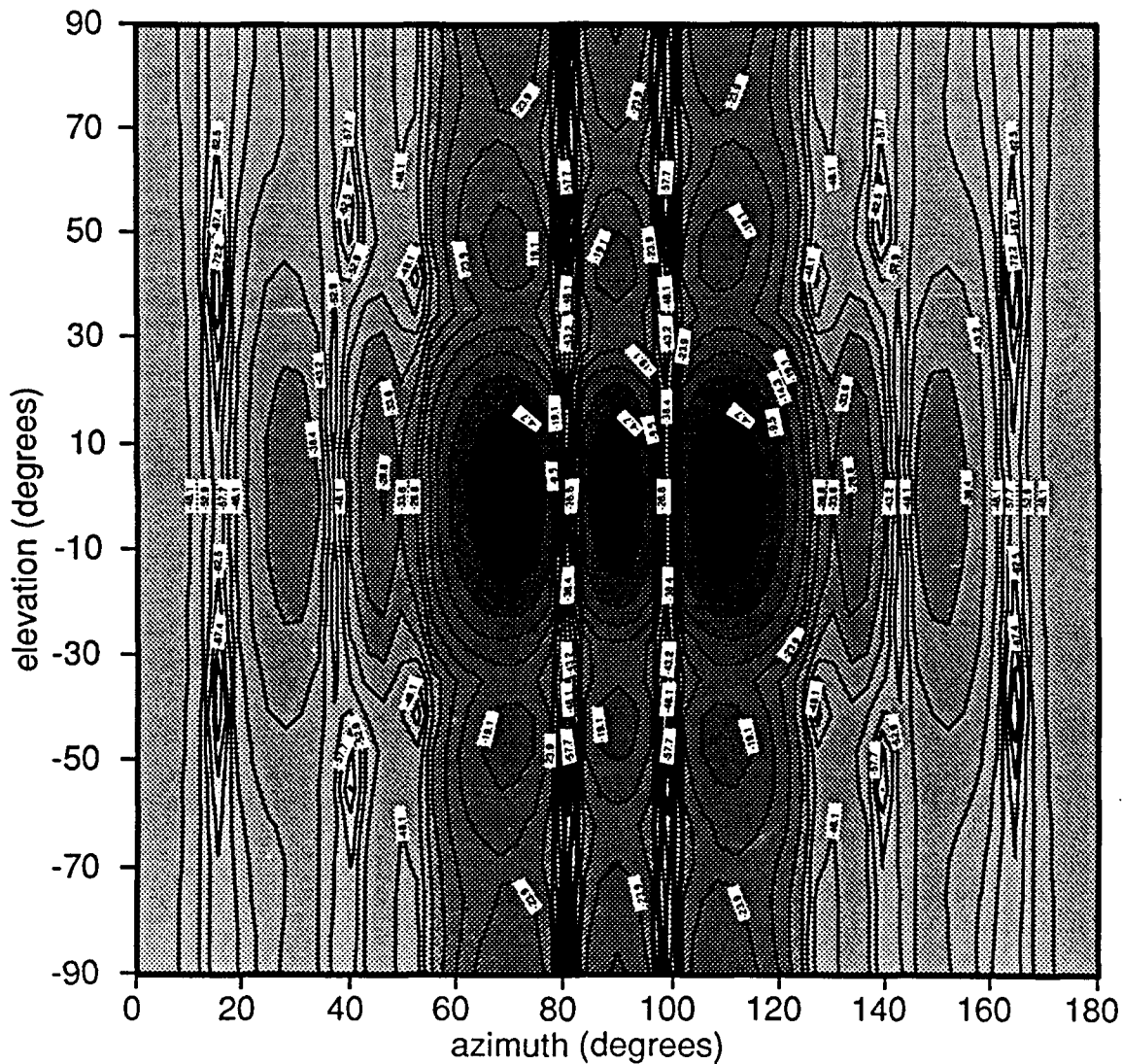


Figure 3-15: beam pattern, case 5B,  $\lambda_{min} = 10^{-4}$

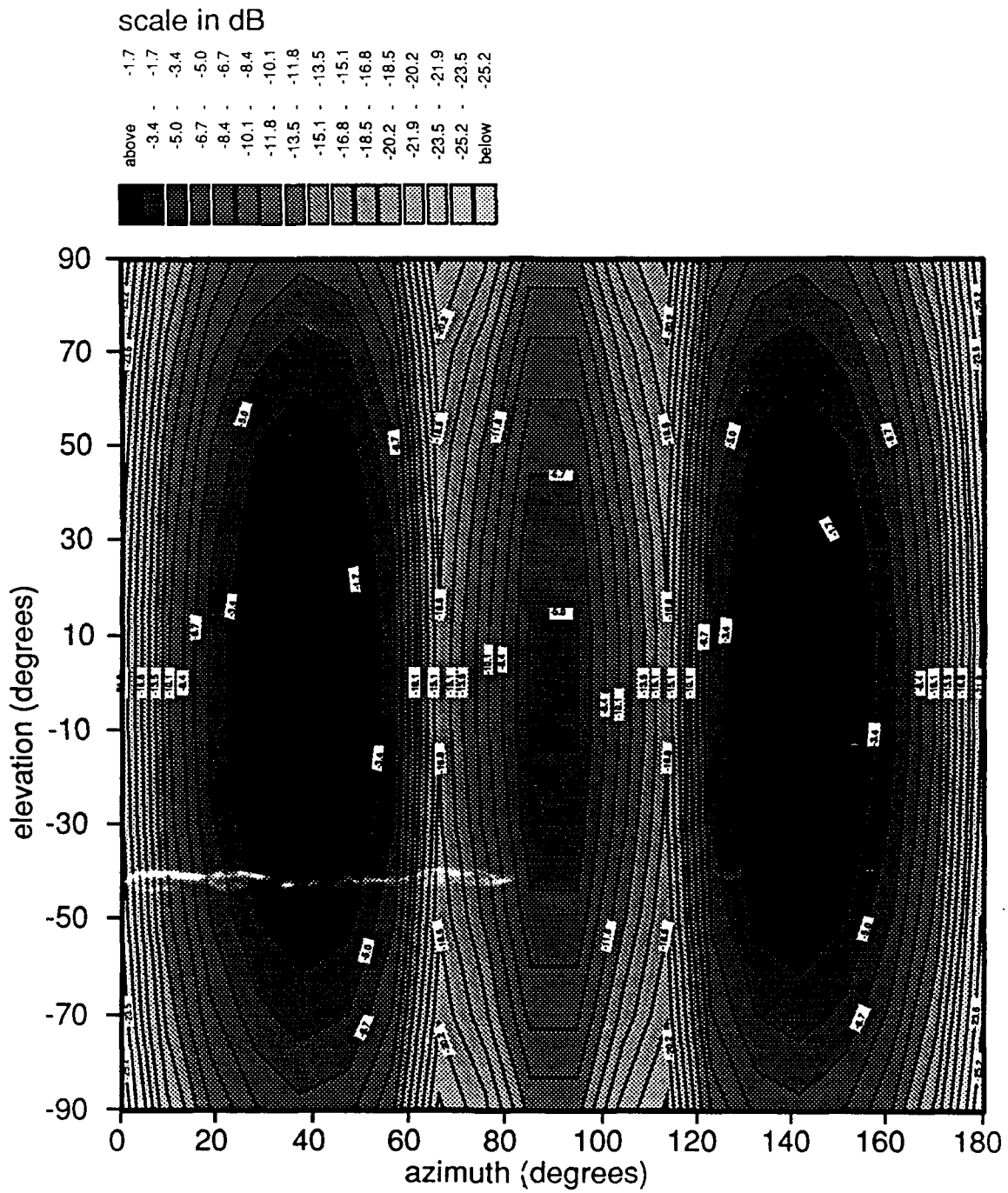


Figure 3-16: square magnitude of element weights, case 5B,  $\lambda_{min} = 10^{-4}$

scale in pi radians

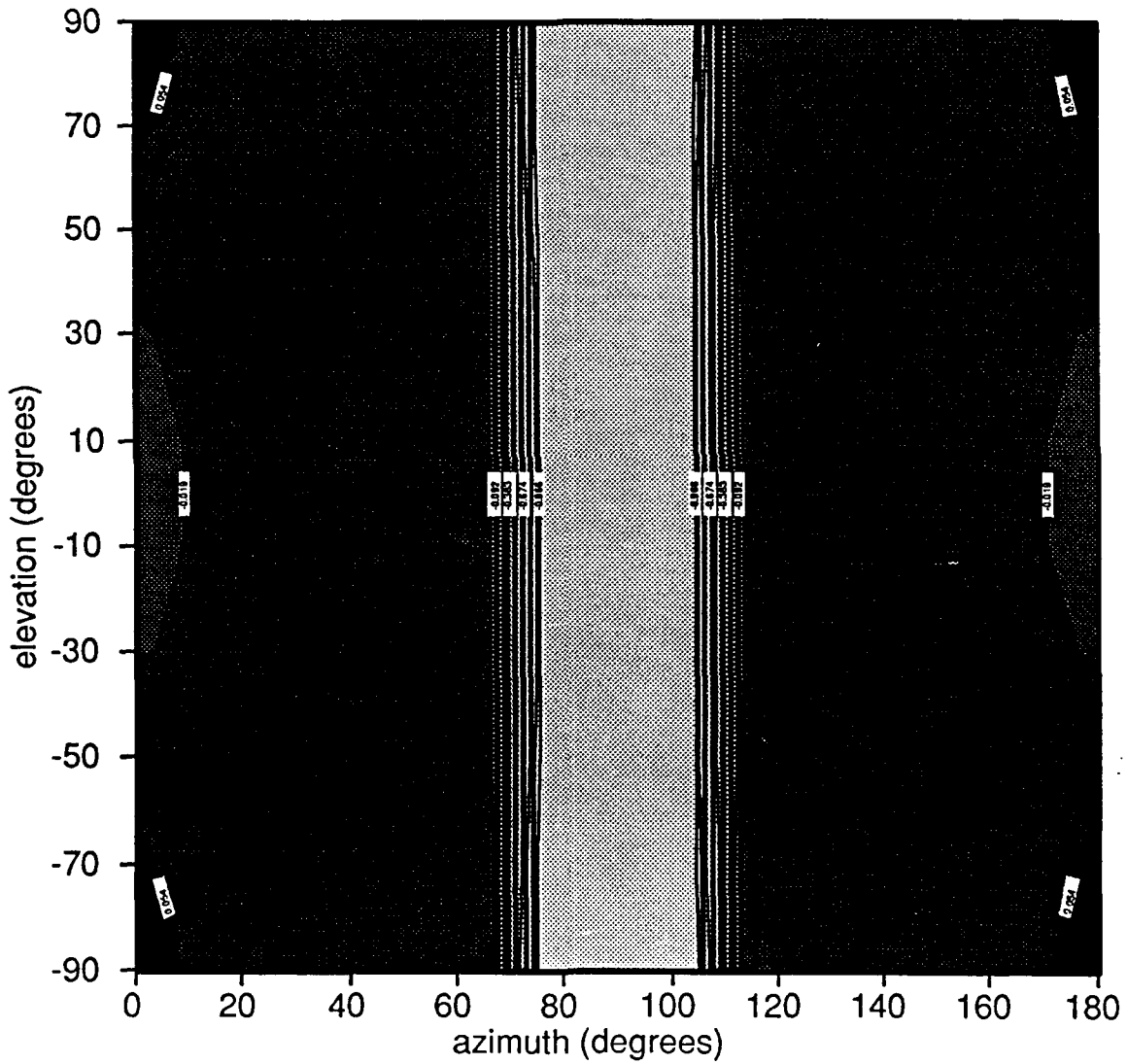
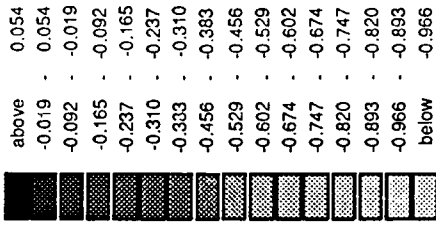


Figure 3-17: corrected phase of element weights, case 5B,  $\lambda_{min} = 10^{-4}$

### 3.3.1 Method A

Virtually no effects due to steers are encountered. When the case 9A penalty function is steered to  $0^\circ$  elevation and  $102^\circ$  azimuth, no distortion of the penalty function in terms of the array output is observed. This is shown in figure 3-18. The really nice feature of the method A procedure is that steering the penalty function has essentially no effect on the sidelobe levels compared to the broadside case. This is shown in figure 3-19. Again, this beam pattern has significantly better sidelobe levels than the steered conventional beam pattern found in figure 3-3. The square magnitude and corrected phase of the element weights for the steered case 9A are shown in figures 3-20 and 3-21. Again, the aperture weights are not characteristic of any traditional shading.

### 3.3.2 Method B

The effects of asymmetry on the method B penalty function are manifested in the concept of edge detections. The asymmetry causes the edges in directions of shorter apertures to be more emphasized which causes a significant sidelobe to be placed in the location of the short aperture edge. This is observed when case 9B is steered to  $0^\circ$  elevation and  $102^\circ$  azimuth; the array is superdirective in this case. As the penalty function center region is made wider and as the array is steered further off broadside, the asymmetry effects become more pronounced. (If the center region is too wide, a threshold effect is again observed where the weights suddenly change character into a dumbbell shape.) The placement of significant sidelobes at the locations of edges is similar to that which is observed for the broadside case 5B. This effect is illustrated by observing the array output and beam patterns for case 5B in figures 3-14 and 3-15 where both edges are emphasized instead of just one edge in the direction of short aperture as is found in the steered case 9B.

Based on these observations, the method B penalty function procedure for steered patterns must be modified. The key is to reduce the center region width to a point where the beamformer cannot distinguish one edge from the other; rather than two nulls in the array output, there appears just one center null. If  $\Delta\phi_c$  is reduced to  $0^\circ$ , then more reasonable results are obtained. The array output, beam pattern and square magnitude

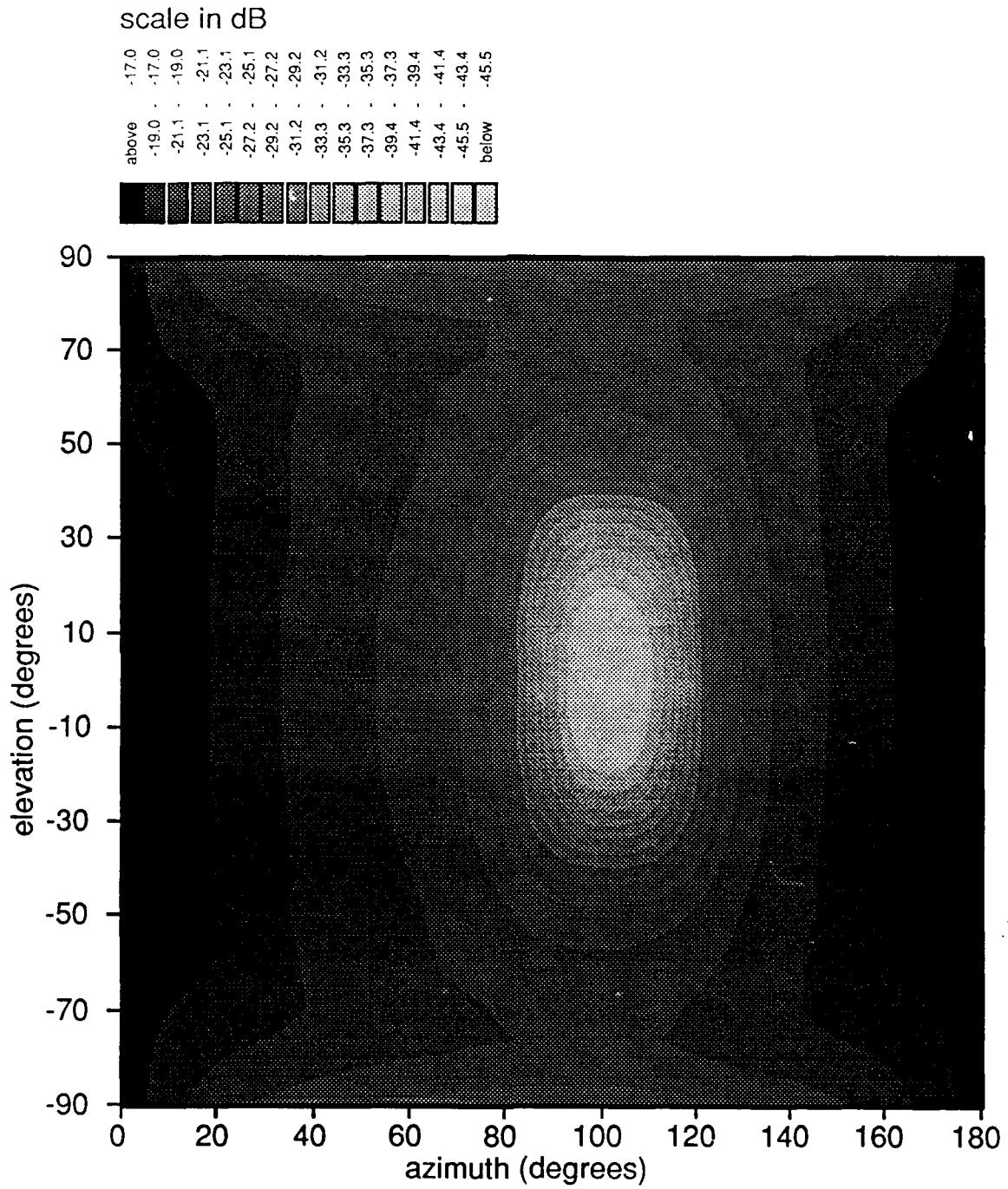


Figure 3-18: array output, steered method A penalty function

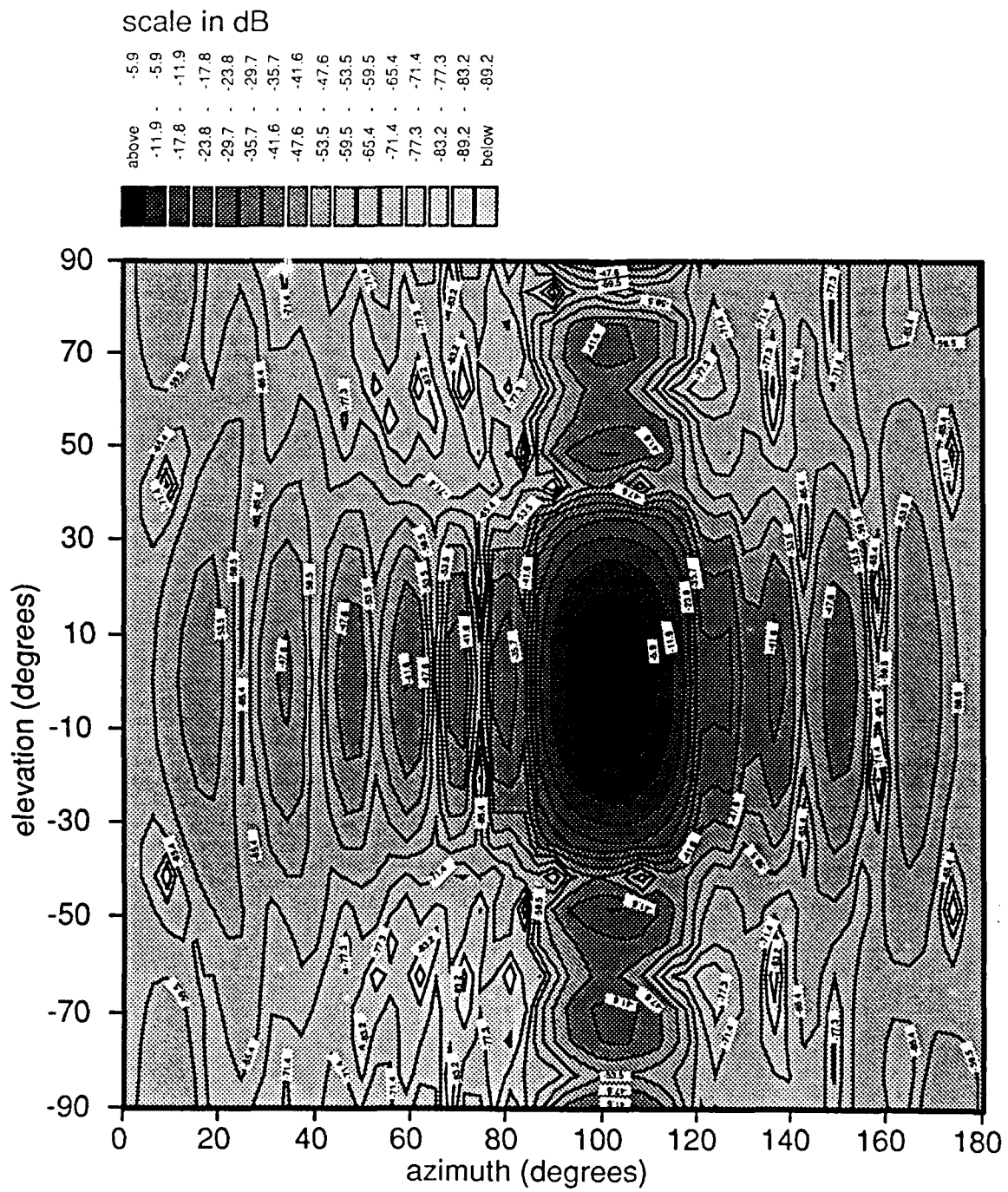


Figure 3-19: beam pattern, steered method A penalty function

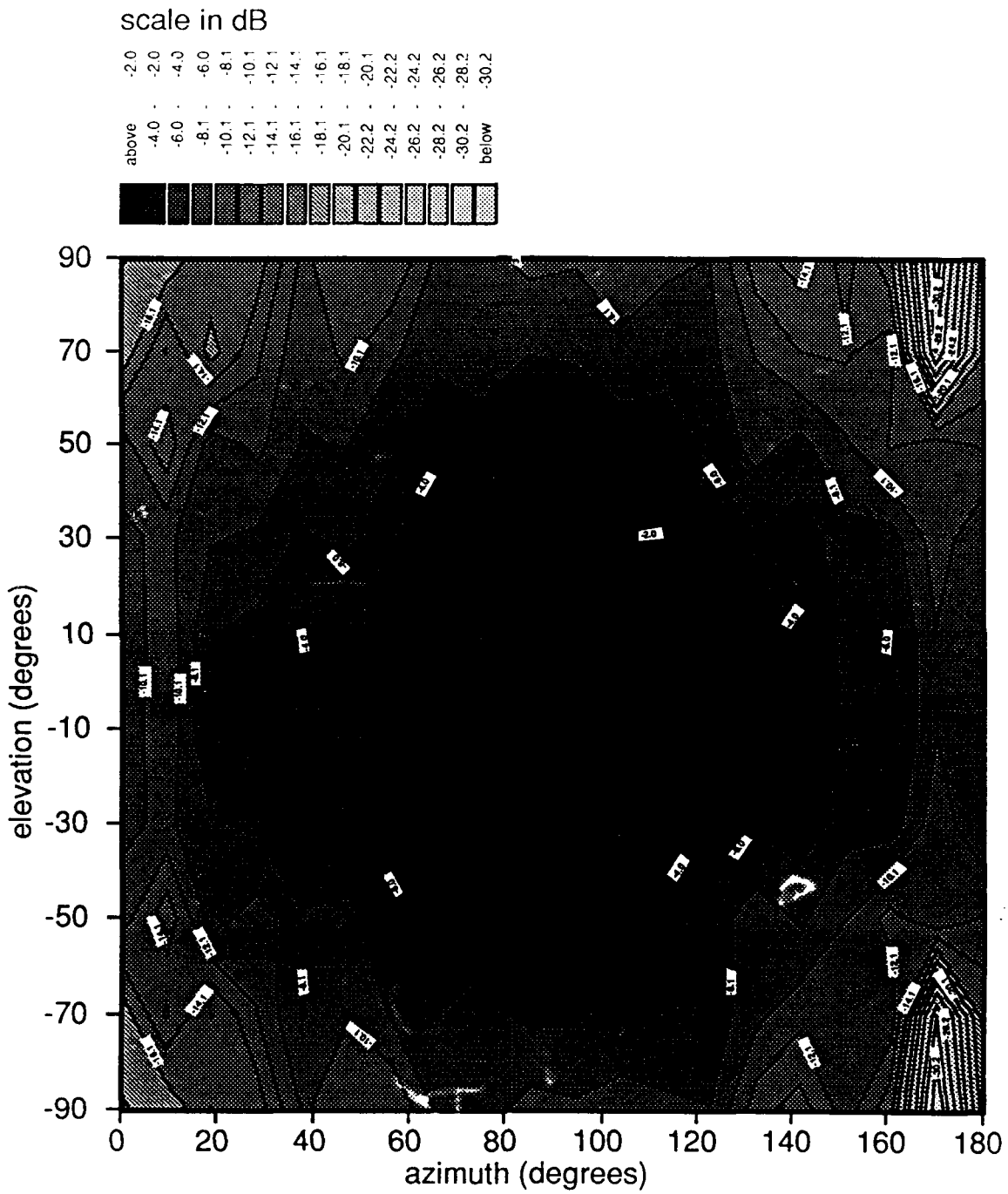


Figure 3-20: square magnitude of element weights, steered method A penalty function

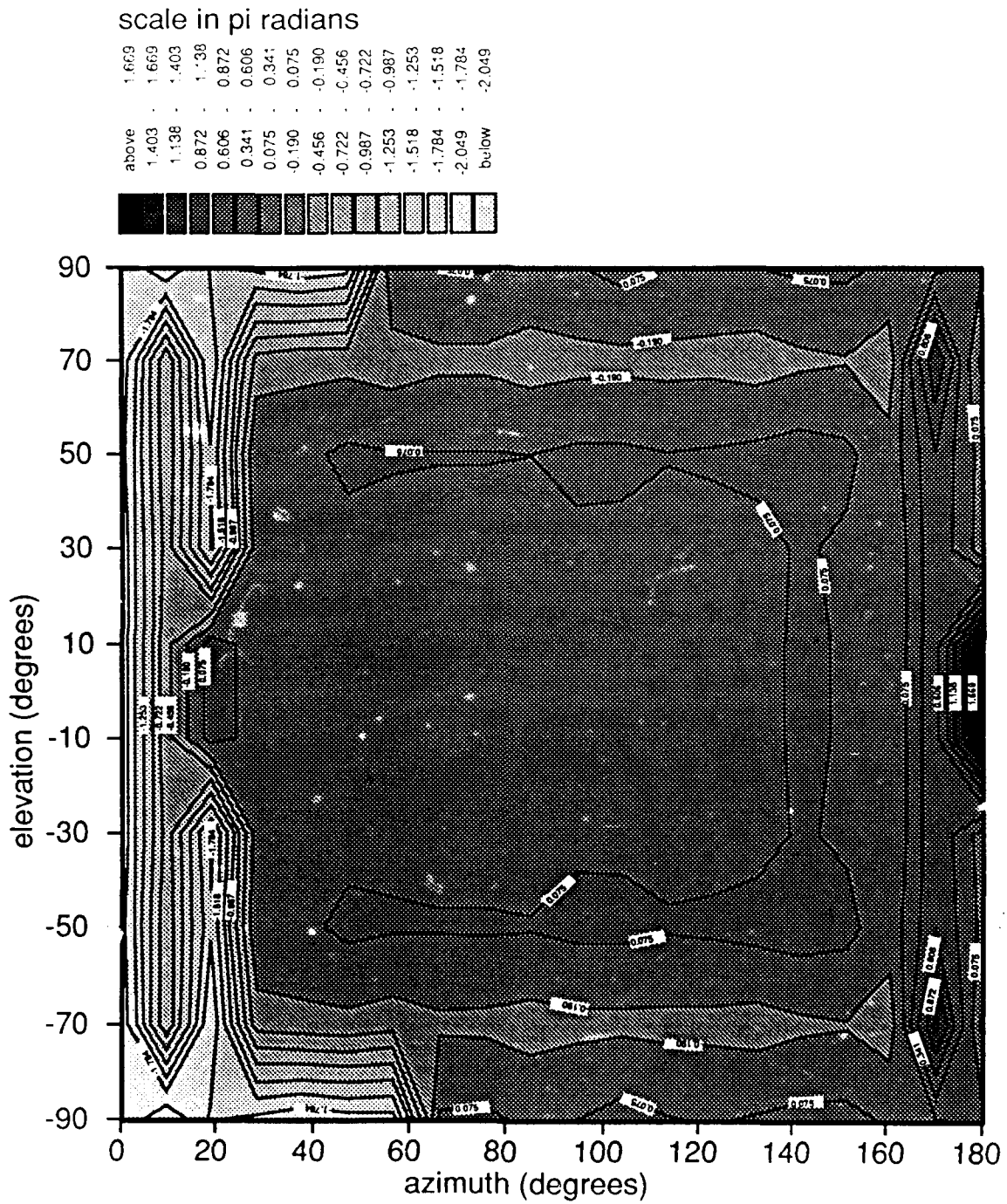


Figure 3-21: corrected phase of element weights, steered method A penalty function

and corrected phase of the element weights for the zero center region width steered to  $0^\circ$  elevation and  $102^\circ$  azimuth are shown in figures 3-22 through 3-25. Although these results are not as good as the broadside case, the beam pattern still has reduced sidelobes compared to the steered conventional beam pattern. Better performance may be obtained if some small center region width is inserted.

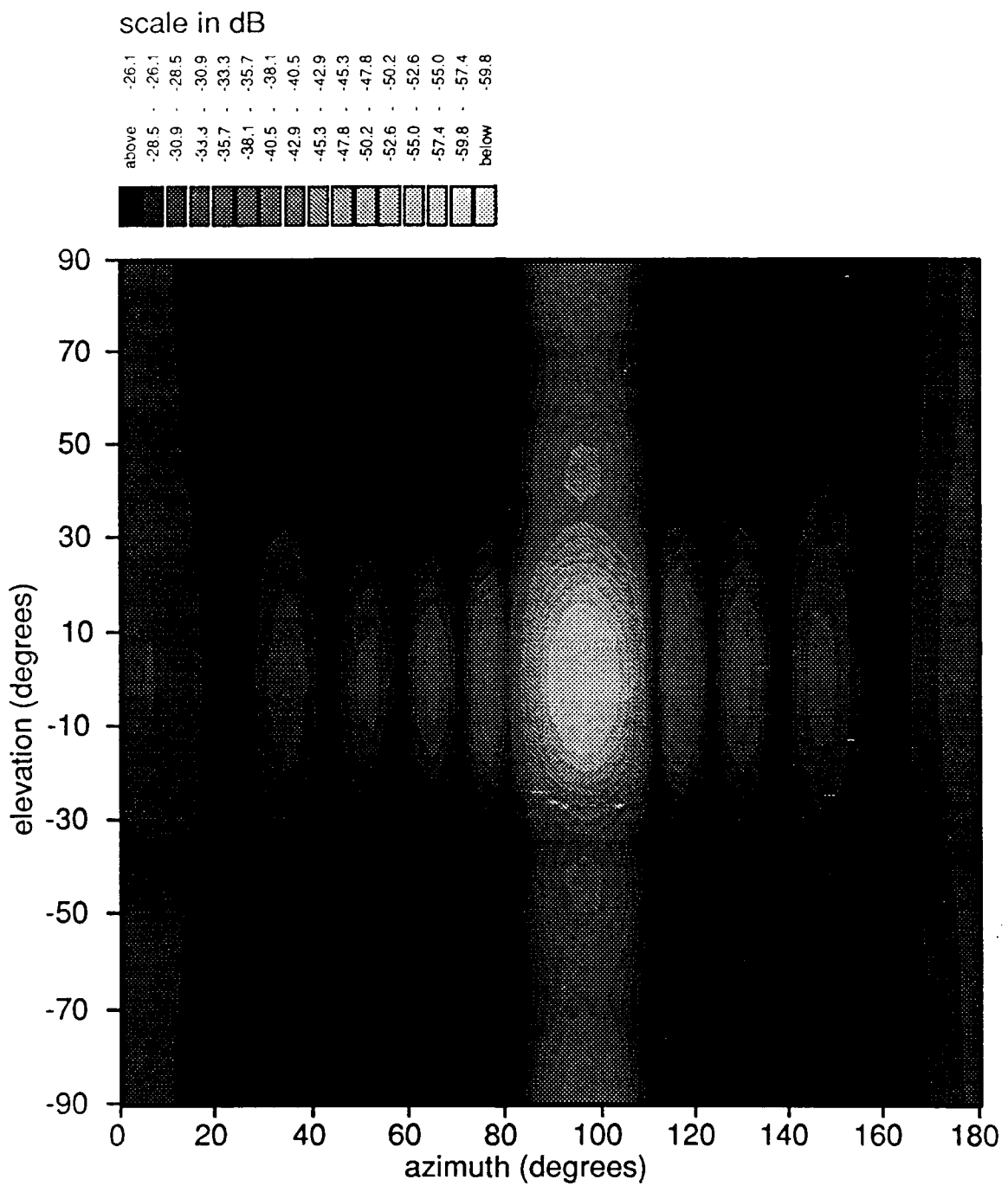


Figure 3-22: array output, steered method B penalty function

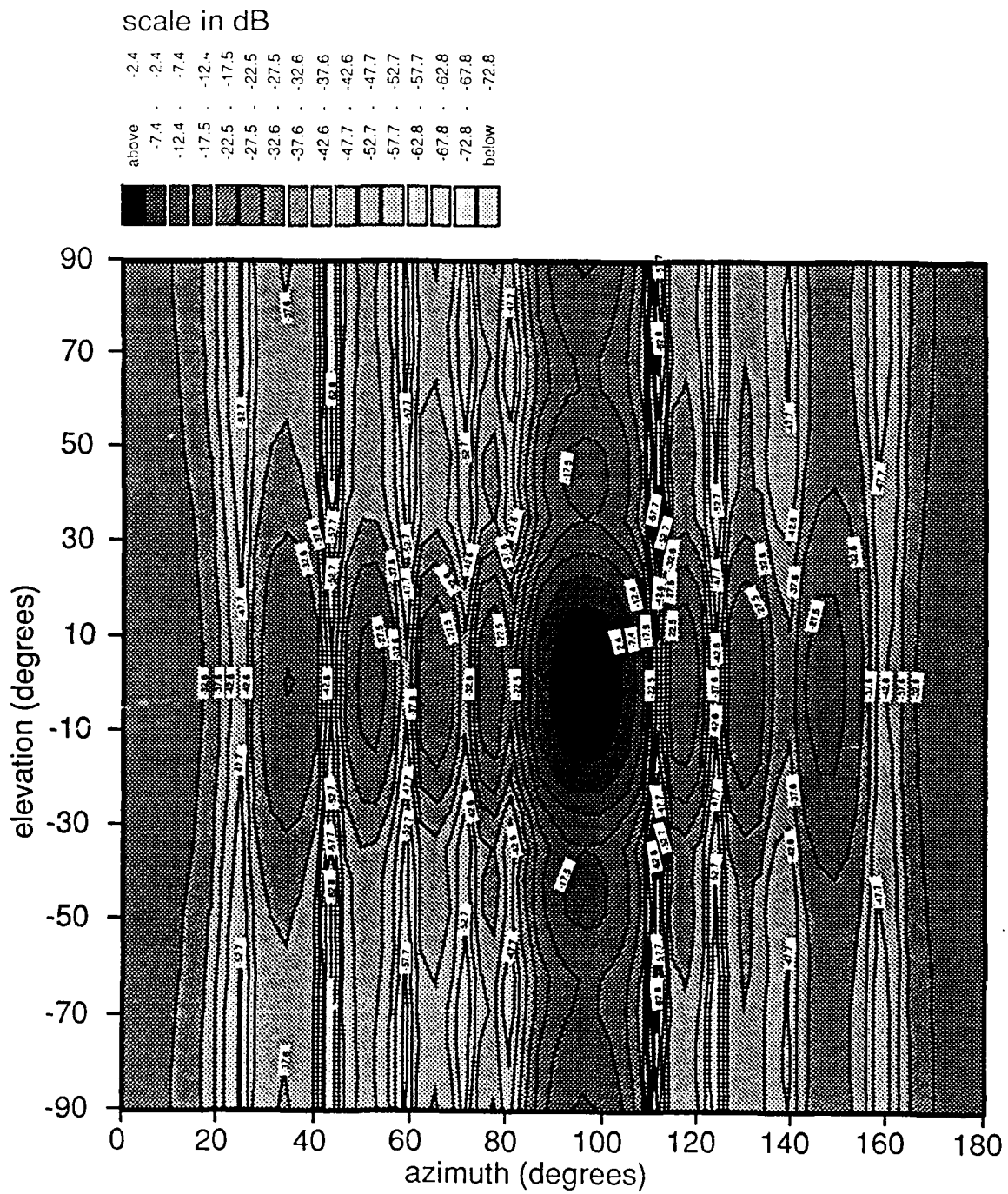


Figure 3-23: beam pattern, steered method B penalty function

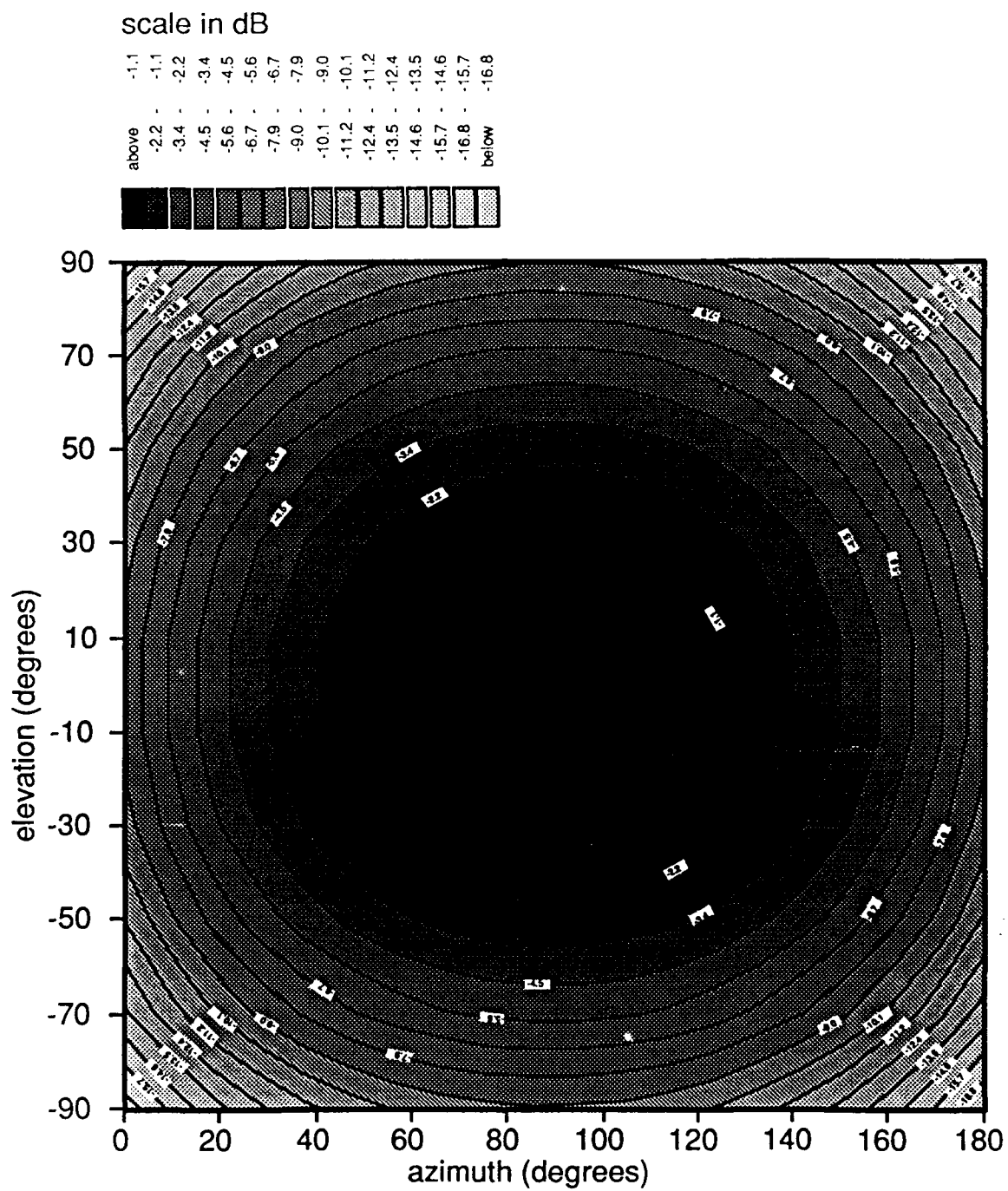


Figure 3-24: square magnitude of element weights, steered method B penalty function

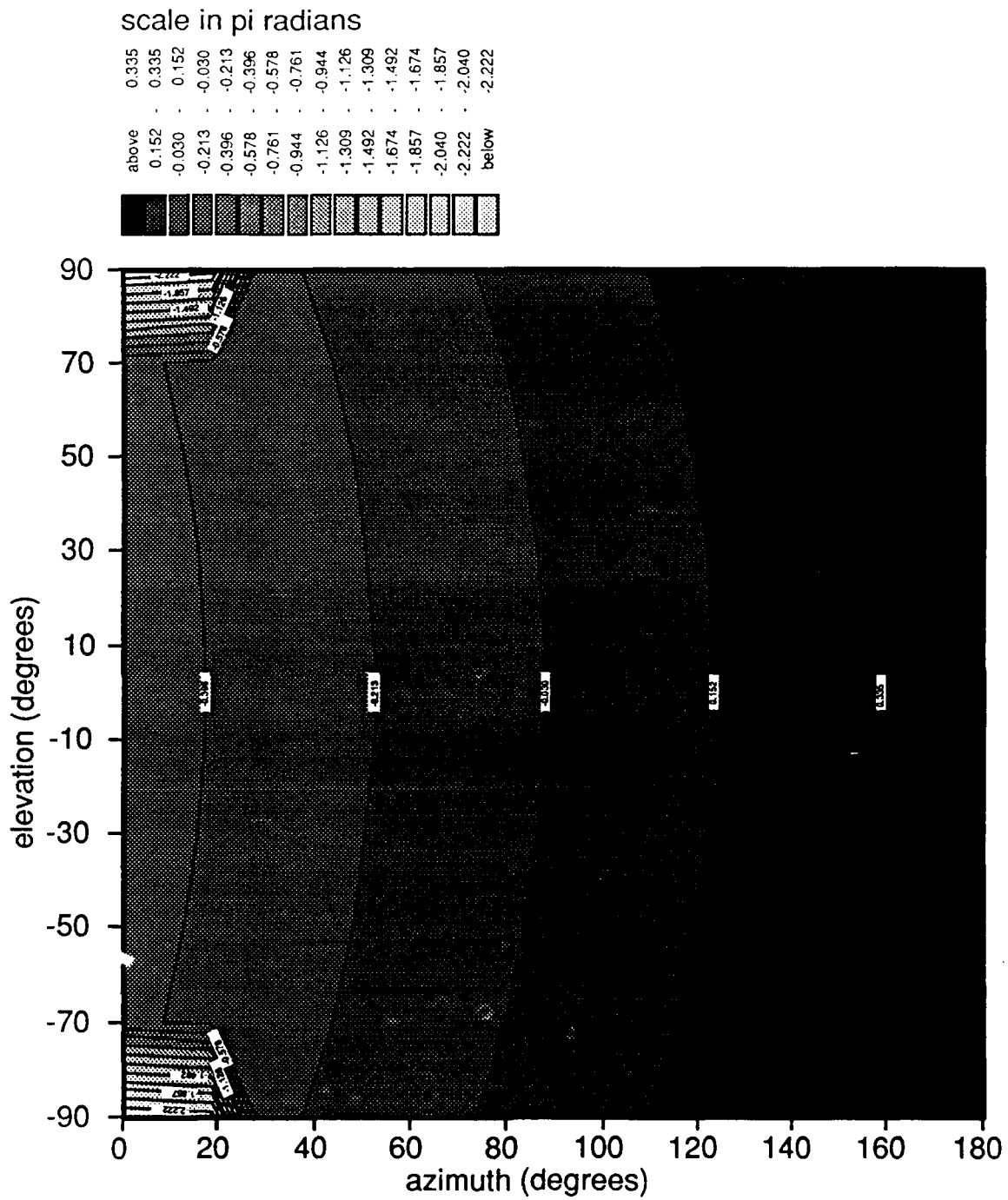


Figure 3-25: corrected phase of element weights, steered method B penalty function

## Chapter 4

# Summary and Conclusions

This investigation features a systematic procedure to design beam patterns for a general multidimensional irregular array, an area where little previous work has been accomplished. The procedure uses a "penalty function" input to an MVDP beamformer. The proper penalty function penalizes high sidelobes and encourages the main lobe. Two different methods of penalty function design are investigated. Method A achieves sidelobe reduction by placing nulls throughout the scanning space encompassing the entire sidelobe region. This method is characterized by fully defining the scanning region; this leads to very predictable and stable performance. Method B achieves sidelobe reduction by emphasizing the main lobe. This is achieved by placing anti-nulls in the main beam region. Method B is characterized by a sparsely defined scanning region; this leads to sometimes unpredictable and unstable performance. The design procedure is a four step process:

1. Determine the main lobe beam width for the conventional beam pattern. The main lobe width is best defined in terms of the angular separation between the first nulls.
2. Select the center region width based on the main lobe beam width and the design method (A or B).
3. Fine tune the effective penalty function width by selecting an appropriate transition region width.

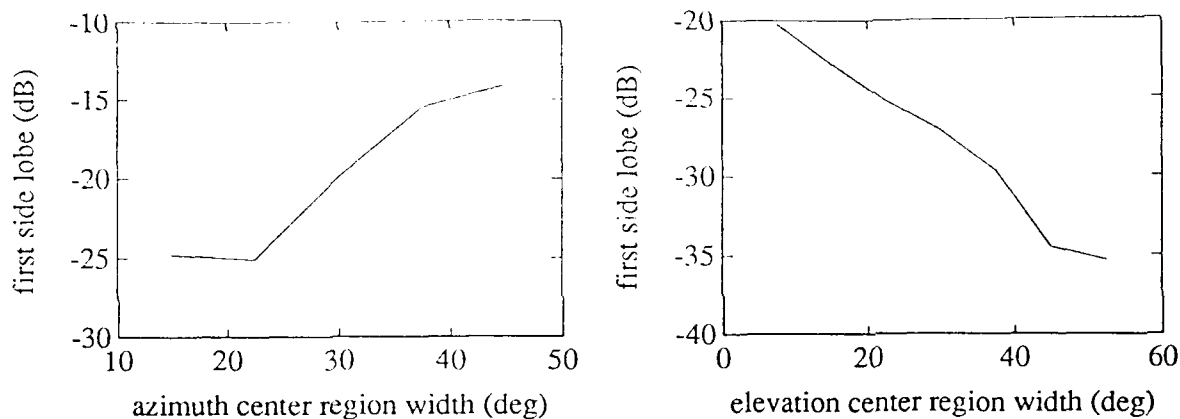


Figure 4-1: Plot of First Sidelobe versus Center Region Width, Method A. Conventional main lobe widths in terms of angular separation between first nulls are approximately  $24^\circ$  in azimuth and  $50^\circ$  in elevation.

4. Stabilize the beamformer by the addition of a sensor noise term in such a way to prevent superdirective performance.

Selection of the center region width is the critical step. There is an optimum center region width with respect to the resultant first sidelobe level. This is illustrated for both methods as applied to the array used throughout the investigation; these results are shown in figures 4-1 and 4-2. The figures show that a minimum in sidelobe level occurs for each direction except in elevation for method A where increasing the center region width eliminates the first sidelobe.

Methods A and B each have distinctive characteristics. The character of each method must be evaluated when considering which method to apply.

- Method A has roughly equivalent sidelobe performance in elevation and azimuth. Method B performance in azimuth is significantly better than performance in elevation.
- In terms of first sidelobe level overall performance in elevation is better with method A; overall performance in azimuth is better with method B.
- Method A results in a narrower main lobe compared to method B which results in better *DI* performance for method A.

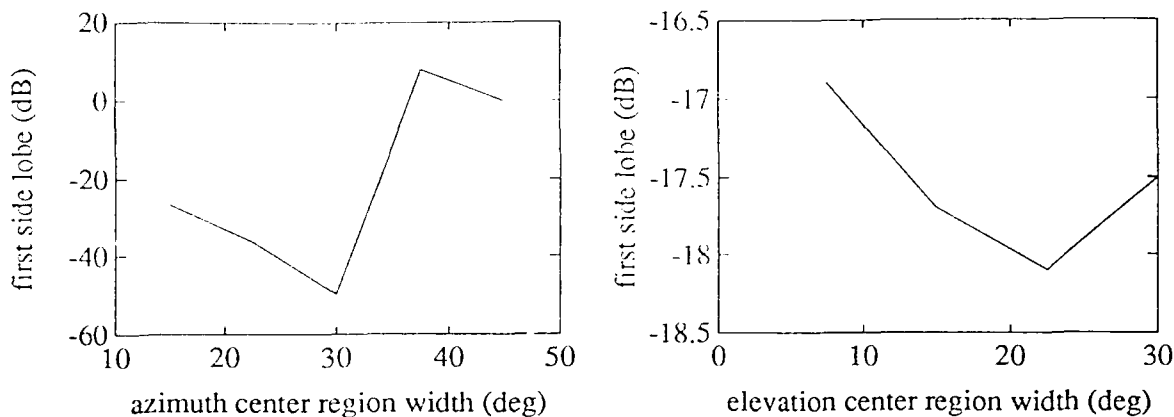


Figure 4-2: Plot of First Sidelobe versus Center Region Width, Method B. Conventional main lobe widths in terms of angular separation between first nulls are approximately  $24^\circ$  in azimuth and  $50^\circ$  in elevation.

- Method A superdirective performance is characterized by high sidelobes in the unobserved  $k$  space. Method B superdirective performance is characterized by high sidelobes in the observable  $k$  space.
- Method A is easily steered; the method B procedure must be modified when steered.
- For method A, azimuth performance is partially coupled to elevation performance. For method B, azimuth performance and elevation performance are uncoupled.
- Method B has stable operating regions where performance is independent of penalty function dynamic range.
- The method B procedure has a threshold effect where the aperture weights suddenly change character from shapes with one global maximum to shapes with two or more local maximum.

The investigation is notably sparse of results for steered arrays; however, with the use of some simple cases, significant sidelobe reduction is achieved for the examined case. Only the effects of steers in azimuth are investigated because of the insensitivity found in elevation. Considering the case presented, the general requirements for steered penalty functions are illustrated.

Additional investigation into several aspects not examined are warranted. Method A is the design method of choice, however, it would be beneficial to obtain sidelobe reduction in azimuth comparable to that found in method B. One proposal to achieve these levels would be the incorporation of a two level background region which more heavily penalizes sidelobes in azimuth.

Finally, one major issue which has been only surficially addressed concerns the robustness or sensitivity of the design procedure in terms of the uncertainty in the amplitudes and phases of the response. This issue is not well understood and yet is so important when characterizing the performance of multidimensional arrays. Further work on this robustness issue is required and is the next step in refining the "penalty function" design procedure.

## Appendix A

# Spectral Covariance Matrix

## Inversion

When considering an MLM beamforming approach, the problem of solving a large system of equations quickly arises. At the outset of this undertaking, it was hoped exploiting the embedded Toeplitz structure of the spectral covariance matrix would lead to significant savings in computational time. What follows are the results of the investigation into Toeplitz matrix inversion techniques.

Consider the matrix problem

$$\mathbf{Ax} = \mathbf{b} \tag{A.1}$$

where  $\mathbf{A}$  and  $\mathbf{b}$  are known. The standard matrix solution method which solves any nonsingular system is Gaussian elimination.[24] The method is well documented and numerous algorithms are readily available which efficiently incorporate the method, particularly the LINPACK routines.[12] The problem with this method is that it is generally the slowest of the standard methods. For an  $n$  by  $n$  real matrix, the number of multiplications for the Gaussian elimination method is proportional to  $n^3$ . A Toeplitz inversion method using a more efficient bordering method was developed by Levinson with the number of multiplications proportional to  $n^2$ . [8] The goal was to incorporate these savings into the more complicated structure of the spectral covariance matrix.

The multidimensional beamforming problem produces a more complicated matrix

scanning pattern	method	time(sec)
aggregate pattern	Gaussian elimination	4400
	Toeplitz	4950
single scan	Gaussian elimination	265
	Toeplitz	160

Table A.1: Computational Times for Matrix Solution Methods

structure as discussed in chapter 2.2.2. Two level Toeplitz matrix solution methods suitable for this complicated matrix structure have been developed.[25,13] The method used is from the Toeplitz Package Users Guide.[13] The number of multiplications for a real matrix with this method is approximately  $2M^3L^2$ . For the particular array structure,  $M = 10$  and  $L = 20$ . This represents a factor of 10 savings from the Gaussian elimination method with  $n = 200$ . Even with the overhead resulting from the permutations required to obtain the proper structure for input into the Toeplitz algorithm, a significant savings is expected. Two factors have not been accounted for up to this point. One, the matrices are complex. Two, the system of equations needs to be solved 1593 times.

The two methods were tested against each other with a 1600 scanning direction pattern, where 1600 vice 1593 scanning directions were used to accommodate permutations of the right hand side of equation A.1, consistent with the permutation of **A**. The timing results were obtained on a Digital Microvax II computer system. The run times for all scanning directions and for just one scanning direction are summarized in table A.1. Although the actual beamforming was performed on an Alliant FX40 computer system, the time performances for both methods were similar.<sup>1</sup>

The superior performance of the Gaussian elimination method for the full problem can be attributed to the LU decompositon method used. Considering the single run times, the full Toeplitz procedure is dependent on **b** and must be repeated for each new right hand side vector. Only a portion of the Gaussian elimination procedure is dependent on **b**. The matrix decomposition need only be accomplished once while the back substitution using the different right hand side vectors can be applied to the same decomposition.

---

<sup>1</sup>No individual run times were examined on the Alliant, only aggregate times. The Alliant times were approximately 65 times faster than the Microvax.

In conclusion, the Toeplitz method is more efficient when the matrix problem only requires a few right hand side vectors; Gaussian elimination is more efficient when a large number of right hand sides must be evaluated.

## Appendix B

# Dolph-Chebyshev Weights

Aperture weights have been presented for method A and method B penalty functions. As previously noted, method A aperture weights have no apparent special structure, but method B aperture weights have a structure which may be compared to a conventional weight. Since the MVDP beamformer is optimum in the minimum variance sense, a useful comparison might be made with Dolph-Chebyshev weights which are optimum in the relationship between minor lobe level and main lobe width. Using the procedures outlined in reference [26], the aperture weighting for a uniform rectangular array can be calculated with input parameters of side-lobe height in both azimuth and elevation. The results for -60 dB side-lobes in azimuth and -22 dB side-lobes in elevation are shown in figure B-1. The Dolph-Chebyshev aperture weights in figure B-1 are remarkably similar to the aperture weights for case 9B in figure 3-12, particularly away from the edges of the array. Furthermore, the side lobe levels for the case 9B beam pattern in figure 3-11 can be characterized by -60 dB in azimuth and -22 dB in elevation. Based on these results, method B penalty function aperture weights can be favorably compared to Dolph-Chebyshev aperture weights.

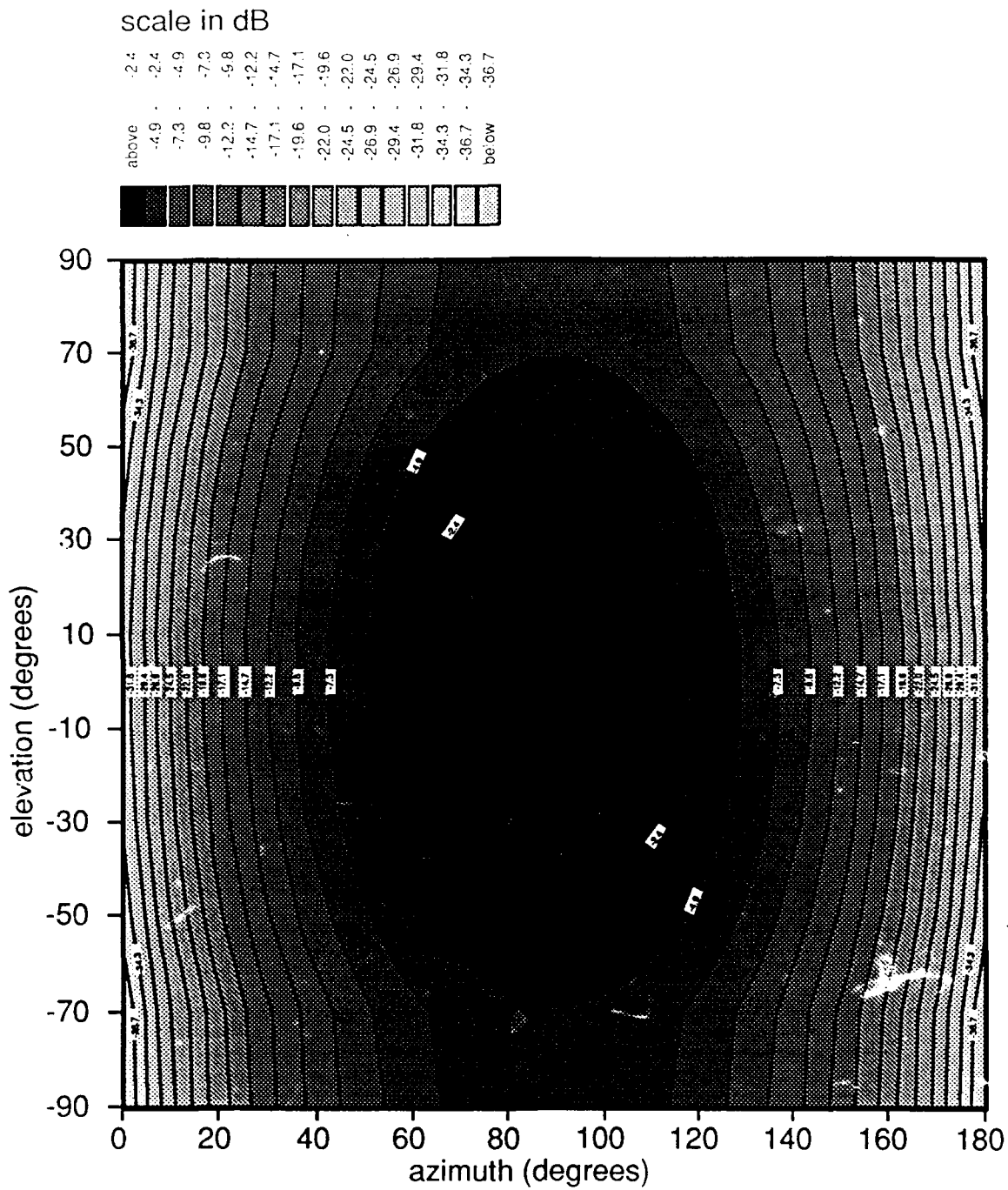


Figure B-1: Dolph-Chebyshev square magnitude element weights

# Bibliography

- [1] A.B.Baggeroer, *Space/Time Random Processes and Optimum Array Processing* (Technical Report TP 506, Naval Undersea Center, San Diego, CA 1976).
- [2] F.J.Harris, "On the Use of Windows for Harmonic Analysis with the Discrete Fourier Transform," *Proceedings of the IEEE* **66**, 51-83 (1978).
- [3] J.H.McClellan, "Multidimensional Spectral Estimation," *Proceedings of the IEEE* **70**, 1029-1039 (1982).
- [4] D.E.Dudgeon, "Fundamentals of Digital Array Processing," *Proceedings of the IEEE* **65**, 898-904 (1977).
- [5] J.H.McClellan, "The Design of Two-Dimensional Digital Filters by Transformations," in *Proceedings of the 7th Annual Princeton Conference on Information Sciences and Systems*, 247-252 (1979).
- [6] D.H.Johnson, "The Application of Spectral Estimation Methods to Bearing Estimation Problems," *Proceedings of the IEEE* **70**, 1018-1028 (1982).
- [7] J.Capon, "High-resolution frequency-wavenumber spectrum analysis," *Proceedings of the IEEE* **57**, 1408-1418 (1969).
- [8] N.Levinson, "The Wiener RMS Error Criterion in Filter Design and Prediction," *Journal of Mathematics and Physics* **25**, 262-278 (1947).
- [9] A.Papoulis, *Probability, Random Variables, and Stochastic Processes* (McGraw-Hill, Inc., New York, NY, 1984), 2nd ed.
- [10] J.Doob, *Stochastic Processes*. (John Wiley and Sons, New York, NY, 1953).
- [11] S.L.Marple, Jr., *Digital Signal Analysis with Applications* (Prentice-Hall, Englewood Cliffs, NJ, 1987).
- [12] J.J.Dongarra, C.B.Moler, J.R.Bunch, and G.W. Stewart, *LINPACK User's Guide* (SIAM, Philadelphia, PA, 1979).
- [13] O.B.Arushanian, M.K.Samarin, V.V.Voevodin, E.E.Tyrtshnikov, B.S.Garbow, J.M.Boyle, W.R.Cowell, and K.W.Dritz, *The Toeplitz Package Users' Guide* (Argonne National Laboratory Report Anl-83-16, Argonne, IL, 1983).

- [14] S.M.Kay and S.L.Marple, Jr., "Spectrum Analysis—A Modern Perspective," *Proc. IEEE* **69**, 1380-1419 (1981).
- [15] A.B.Baggeroer, W.A.Kuperman, and H.Schmidt, "Matched Field Processing: Source Localization in Correlated Noise as an Optimum Parameter Estimation Problem" *J. Acoust. Soc. Am.* **83**, 571-587 (1988).
- [16] G.L.Duckworth, *Adaptive Array Processing for High Resolution Acoustic Imaging* (S.M. and E.E. Thesis, Department of Electrical Engineering and Computer Science, MIT, Cambridge, MA, 1980).
- [17] H.Cox, "Resolving Power and Sensitivity to Mismatch of Optimum Array Processors," *J. Acoust. Soc. Am.* **54**, 771-785 (1973).
- [18] H.Cox, R.M.Zeskind, and M.M.Owen, "Robust Adaptive Beamforming" *IEEE Transactions on Acoustics, Speech, and Signal Processing ASSP-35*, 1365-1375, (1987).
- [19] A.V.Oppenheim and R.W.Schafer, *Discrete-Time Signal Processing* (Prentice-Hall, Inc., Englewood Cliffs, NJ, 1987).
- [20] I.Dyer, *Fundamentals and Applications of Underwater Sound* (Course Notes for 13.851, Ocean Engineering Department, MIT, Cambridge, MA, Spring 1989).
- [21] B.T.Smith, J.M.Boyle, J.J.Dongarra, B.S.Garbow, Y.Ikebe, V.C.Klema, and C.M.Molar, "Matrix Eigensystem Routines—EISPACK Guide," in *Lecture Notes in Computer Science*, edited by G.Goos and J.Hartmanis (Springer Verlag, New York, NY, 1976).
- [22] W.E.Boyce and R.C.Diprima, *Elementary Differential Equations and Boundary Value Problems* (John Wiley and Sons, New York, NY, 1977), 3rd ed.
- [23] R.J.Urick, *Principles of Underwater Sound* (McGraw-Hill, New York, NY, 1983).
- [24] G.Strang, *Introduction to Applied Mathematics* (Wellesley-Cambridge Press, Wellesley, MA, 1986).
- [25] H.Akaike, "Block Toeplitz Matrix Inversion" *SIAM Journal of Applied Mathematics* **24**, 234-241 (1973).
- [26] N.Davids, E.G.Thurston, and R.E.Mueser, "The Design of Optimum Directional Acoustic Arrays," *J. Acoust. Soc. Am.* **24**, 50-56 (1952).